FIRST DIGITAL FORELIMB RECONSTRUCTION AND RANGE OF MOTION ASSESSMENT OF THE LATE CRETACEOUS DINOSAUR *TROODON FORMOSUS*

by

Michael Anthony Serio

A thesis submitted in partial fulfillment
of the requirements for the degree

of

Master of Science

in

Earth Science

MONTANA STATE UNIVERSITY
Bozeman, Montana

May 2023

ACKNOWLEDGEMENTS

I would first like to thank my committee members for their guidance, and flexibility throughout the last two years. Dr. David Varricchio was instrumental in shaping the questions and principles guiding the project. He's also helped reign in my curiosity when I go in too many directions. Dr. Ashley Heers' guidance, especially creating joint coordinate systems, has been invaluable. This project wouldn't be the same without her expertise. Dr. John Scannella pushed the questions behind this project, expanding what I thought possible. Afterall, the key to good research is a good question! Special thanks to the Museum of the Rockies staff, Eric Metz and Lee Hall for collections access and help using their scanner. Thanks to the Canadian Museum of Nature, Dr. Scott Rufolo, Dr. Jordan Mallon and Alan McDonald, who provided scans of *Latenivenatrix*. Dr. Jingmai O'Connor helped hone my abstract. Dr. Corey Pew explained the math behind joint coordinate systems. Dr. Armita Manafzadeh for clarifying how digital joint creation works. To my friend Tim Trenkle, who's assistance with Blender made data acquisition astronomically faster. Eric Przybyszewski, who's video card kept my computer alive. Eric Gardner, who's own research provided inspiration and connection for my own. To Mom and Dad, who've supported and inspired me throughout all life's twists and turns. And the late Dr. Dale Russell, who dared to consider that these animals were up to something more.

Funding for this project is provided by the Jack Horner Paleontology Scholarship, graciously donated by Gerry Ohrstrom, and a Paleontological Society Student Research Grant. Specimens were collected on land owned by the Blackfeet Nation, as well as the families of Lewis Carroll, Vernon Carroll, and Huey Monroe. Specimens were collected with the help of an NSF grant awarded to Jack Horner.

TABLE OF CONTENTS

TABLE OF CONTENTS, CONTINUED

LIST OF TABLES

Table Page

LIST OF FIGURES

Figure Page

ABSTRACT

Troodon formosus (*Troodon*) is a theropod dinosaur from the Late Cretaceous of North America primarily known from fragmentary fossil material. Hypothesized to hunt small game, *Troodon*, like many theropods, may have actively engaged its forelimbs to aid hunting behavior. Furthermore, the complexity of preserved nests associated with *Troodon* suggest it had sufficient range of motion and dexterity to use its forelimbs to manipulate its eggs. Additionally, *Troodon's* evolutionary position as one of the closest groups to living birds could indicate important information about the evolution of the avian wing. However, no complete forelimb material has yet been found for *Troodon*, and as such a complete reconstruction and range of motion (ROM) estimate of its forelimbs has yet to be attempted. This study aims to address these hypotheses and shortcomings by leveraging recent digital modelling technology to create the first forelimb reconstruction and ROM for *Troodon*.

To overcome preservation limitations, surface scans from multiple *Troodon* fossils housed in the Museum of the Rockies (Bozeman, Montana) were digitally combined to reconstruct most of a forelimb. From this model, digital articulation in the software package Maya was compared with physical articulation ROM methods using 3D printed copies of the forelimb. The maximum angle of allowed motion for each forelimb joint until bone-on-bone contact was assessed.

Results show increased flexion over extension in *Troodon's* joints, consistent with closely related species. However, *Troodon* also shows higher manual extension than close relatives. The humerus is also shorter and stockier, showing mechanical specialization for strength vs speed, and convergent features with primitive theropod species. These ROM and morphological differences imply a deviation in hunting strategy or forelimb utility and a deviation from avian forelimb morphology. Total manual ROM results cannot confirm whether *Troodon* was able to grasp its eggs and small prey single-handed, but two-handed apprehension remains feasible.

This study utilized digital and physical ROM methods, analyzing for the first-time specimens that would have been previously overlooked. These results shed light on both the foraging and reproductive behavior of *Troodon* and have implications for understanding the evolution of modern avian reproductive behavior and the dinosaur-bird transition.

INTRODUCTION

Troodon formosus (*Troodon*) was first discovered in 1855 by geologist Ferdinand Hayden during a geological survey of the Judith River in the Nebraska territory, in what is known today as Montana. A single tooth was discovered in what would later be known as the Judith River Formation and sent to Joseph Leidy in Philadelphia. In 1856 the tooth was described and given the name *Troodon formosus, Troodon* meaning, 'wounding tooth' (Leidy, 1860). Among the other fossils collected by Hayden and described by Leidy, *Troodon,* was one of the earliest dinosaur fossils described in North America. Initially assigned by Leidy as a lacertilian reptile, in the early 1900's *Troodon* was reassigned by Franz Nopcsa as a dinosaur but was put in the largely undifferentiated group, megalosauridae (Nopcsa, 1901). In 1924 Charles W. Gilmore described a mandible from a pachycephalosauridae, originally assigned as *Stegoceras.* Based on its tooth and mandible morphology Gilmore assigned *Stegoceras* as being synonymous with *Troodon* (Gilmore, 1924). This classification stood until 1945, when Charles Sternberg re-assigned *Troodon*, finally recognizing the material as belonging to a small theropod (Sternberg, 1945). Prior to this, in 1932, Sternberg described a theropod named *Stenonychosaurus inequalis* based on isolated pes (Sternberg, 1932). In 1986 work by Phil Currie linked *Troodon formosus* and *Stenonychosaurus inequalis,* making *Stenonychosaurus* the junior synonym to *Troodon* (Currie, 1987). The discussion regarding the validity and placement of *Troodon* is ongoing, with a new proposition put forth in 2017 to synonymize *Troodon* material from Dinosaur Park in Alberta as the junior synonym to *Stenonychosaurus* (Van der Rees and Currie, 2017). For the purposes of this thesis, all troodontid material collected from the Two Medicine formation of Montana is being assigned to *Troodon* as the senior synonym of *Stenonychosaurus*.

Throughout the 1990's new material for *Troodon* was again discovered in Montana, but this time outside the Judith River, in The Two Medicine Formation. The Two Medicine Formation is a series of sediment deposits shed from the ancestral Sevier Mountain range during the Cretaceous and deposited into low coastal plains bordering the Western Interior Seaway (McGookey, 1972; Gill and Cobban, 1973). The Two Medicine Formation has been dated to within 82 and 75 million years ago (Ma), making it contemporaneous with the Judith River Formation (Ramezani et al., 2022; Rogers et al., 1993; McGookey, 1972; Gill and Cobban, 1973). Most of the *Troodon* specimens referenced in this study within the Two Medicine Formation were found in an assemblage known as Jacks Birthday Site (JBS). JBS is a Late Cretaceous deposit within the upper Two Medicine Formation, dated to 74 Ma and interpreted as a shallow floodplain lake (Rogers, 1992; Varricchio, 1995). Among the numerous dinosaur material found at the site, the most common includes multiple species of hadrosaurs, including *Hypacrosaurus*, *Prosaurolophus* and *Gryposaurus,* tyrannosaurid material, and a relative abundance of isolated *Troodon* material, with the only recorded multi-individual occurrence of any troodontid. With the discovery of *Troodon* nests within the Two Medicine formation in 1993 it was inferred that *Troodon*, like its hadrosaur and bird relatives, made nests (Varricchio et al., 1997). One pair of clutches shows evidence for nesting fidelity, the reuse and potential return to a nesting site either over a breeding season or seasons (Varricchio et al., 2015). Additionally, the clutches attributed to *Troodon* show the elongate eggs oriented at an angle, with the tips pointing toward the center of the nest, and bottoms-oriented outwards, potentially indicating the orientation and manipulation of the eggs post laying. Finally, the presence of gastric pellets bearing mammalian skeletal material were found in the Two Medicine Formation and were

described in 2021, being attributed in that study to *Troodon* (Freimuth et al., 2021). Given the complexity of nest construction observed for *Troodon*, along with the fossil material from JBS, regurgitates from the Two Medicine Formation and previously described material attributed to *Stenonychosaurus,* the image of a gracile, quick, small game hunter with improved eyesight and near avian intelligence has taken form (Russell, 1969; Varricchio et al., 2021).

Considering these adaptations and hypotheses, it has been further hypothesized that *Troodon* would have had rather dexterous hands and mobile arms (Russell and Seguin, 1982). Additionally, considering the proximity of avian birds to Paraves, the group of theropods that includes troodontids, dromaeosaurs and birds, *Troodon*'s evolutionary history could also help inform the evolution of Avialae (Sereno, 1999). Until recently a reconstruction and range of motion has been unfeasible for *Troodon* given a lack of complete associated material collected, so these hypotheses have yet to be addressed. Advances in surface scanning and digital modeling technologies now allow for the accurate digitization and manipulation of physical bones in 3D space. This medium has allowed this project to combine forelimb bones from different individual *Troodon* fossils collected from the JBS and Two Medicine Formation. These bones were mirrored and scaled to create a single forelimb. From this digital reconstruction the range of motion at each available joint was measured in software. These methods, now allow for the assembly of a complete *Troodon* forelimb, helping to test old hypotheses using specimens that have previously been unfit for such analysis.

Range of motion (ROM) studies have long been a focus of paleontological research, (Galton, 1971; Sereno, 1994; Novas and Puerta, 1997; Carpenter, 2002; Senter, 2006b; White et al., 2015; Senter and Sullivan, 2019). Traditionally, ROM studies have been performed with

fossil bones or casts of bones that are physically manipulated through a joint's range of motion. With these studies the maximum mobility of a joint is assumed to be the bone-on-bone contact where the articulated surface of the distal bone will not pass the extent of the articulated surface of the proximal bone (Senter and Corwin, 2019; Yu et al., 2022). For simplicities sake these studies leave out the influence of soft tissues, like cartilage. These traditional studies are less adept at revealing whether a position would be adopted by a living organism but excel at identifying the extent of positions and movements that would have been unrealistic for a particular individual to perform.

Over the last twenty years more studies have been exploring ROM studies via digital means (Mallison, 2010; Baier and Gatesy, 2013; Manafzadeh and Padian; 2018, Herbst et al., 2022), with select studies combining skeletal data with inferred soft tissue reconstruction as well (Burch, 2014; Heers et al., 2018; Bishop et al., 2021). These studies have benefitted greatly from the work of studies performed with living specimens that observe range of motion and soft tissue orientations using x-ray techniques, known as X-ray Reconstruction of Moving Morphology (XROMM; Gatesy et al., 2010; Baier and Gatesy, 2013). The results from these studies have helped confirm long standing assumptions about joint movement that couldn't be experimentally verified. These studies helped confirm that joints exhibit movement in up to six degrees of freedom, and often simultaneously with three rotational: flexion-extension (FE), abduction-adduction (ABAD) and long-axis rotation (LAR), and three translational: medial-lateral translation, anterior-posterior translation, and distraction-compression translation (Kambic et al., 2014; Manafzadeh and Gatesy, 2021). XROMM also revealed how important LAR was to joint function, with small changes in the former having a great effect on the latter (Kambic et al.,

2014). Applying this knowledge to extinct taxa has remained challenging, with the constraints of soft tissues largely being lost, but there is a growing movement to take this data and apply it to extinct groups (Bishop et al., 2021; Manafzadeh and Gatesy, 2022). However, despite the recent advances most digital reconstructions incorporating all six degrees of freedom on extinct taxa have focused on hindlimb studies (Manafzadeh and Padian, 2018; Bishop et al., 2021). Few digital approaches to date have been able to apply the newer methods to forelimb ROM studies, with most still relying on a single angular degree of freedom and utilizing the bone-on-bone approach (White et al., 2015; Senter and Sullivan, 2019). Because of this disconnect there has been little crossover and an understanding of the pros and cons of each approach for forelimb studies has not been formally assessed. This study attempts to understand these pros and cons by performing a digital ROM assessment on an extinct dinosaur forelimb, incorporating as many degrees of freedom as is feasible. Additionally, physical 3D-printed high-fidelity copies of the digitally scanned and scaled bones were used during the modeling process to check the differences and overlap between both the physical and digital methods. It is important to note that this study does not exemplify an exhaustive comparison between both approaches. This study does provide an initial ROM investigation into three out of six degrees of freedom while detailing some of the pros and cons of physical and digital ROM studies.

METHODS AND MATERIALS

Methods

Bone Scanning

Troodon material collected from JBS has black to dark brown coloration. Cranial, axial, and appendicular skeletal elements have been recovered, however no complete skeleton for *Troodon* has yet been found. Articulated material is rather rare and most collected specimens are isolated skeletal elements. Fossils collected from JBS show minimal crushing, and breakage that primarily occurs perpendicular to the length of the element, indicating damage that likely occurred post fossilization. Additional material used for this study was found from the Blacktail Creek locality within the Two Medicine Formation (MOR locality TM-071). Specimens referenced from Blacktail Creek include nearly all forelimb elements, and are from a partially articulated, incomplete individual, but are more corroded relative to JBS material. Only one bone from Blacktail Creek was used in the final forelimb reconstruction, its use is detailed in Table 1 below.

While a complete *Troodon* forelimb has not yet been found, there is enough material collected from the Two Medicine sites that represents most of a forelimb. Forelimb material includes the scapula, partial coracoid, humerus, broken ulna, partial radius, semilunate carpal, metacarpals, phalanges and ungual bones. The only bones completely missing from the reconstruction include two phalangeal bones from the third digit (III) and the radiale. In total there were sixteen bones used in the reconstruction, representative of at least 4 individuals. All the bones used in this study are accessioned at the Museum of the Rockies (MOR, Bozeman, MT), with most elements coming from MOR 553 collected from JBS, and additional elements

from MOR 563 collected from Blacktail Creek. For a complete listing of elements used in this study see Table 1.

Selected forelimb elements were scanned at the MOR using a Creaform GO! Surface 3D scanner (AMETEK Inc.) at a 0.30 mm resolution. Two scans, a distal and proximal of each element, were initially made and then both were combined into one digital element. The single element was cleaned using VXelements 3D software and saved as an .STL file. Completed .STL files were then imported into the 3D animation software, Maya (Autodesk) and saved in the .OBJ file format. To match the left side material, right sided forelimb elements including the scapula, coracoid, humerus, and metacarpal-I were mirrored. Once scanned and mirrored, the selected digital elements were scaled to form a single left forelimb, as detailed below.

Table 1: *Troodon* Forelimb Elements Used in This Study

***Troodon* Forelimb Specimens**						
Museum #	**Field #**	**Specimen ID**	**Mirrored**	**Scaling***	**Scaling Certaintity**	**Notes**
MOR 553 S	7.24.91.196	Scapula	Yes	Up-scaled	More Certain	Scaled from greatest distal width
MOR 553 S	2021-c-182	Coracoid	Yes	Up-scaled	More Certain	Scaled to match scapula
MOR 553 S	8.2.92.303	Humerus	Yes	N/A	N/A	Distal condyles modified based on 7.19.0.96
MOR 553 S	7.19.0.96	Humerus	No	N/A	N/A	Used as reference for 8.2.92.303
MOR 553 S	8.12.92.219	Ulna	No	Up-scaled	More Certain	Ulna was broken, had to be merged into one mesh
MOR 553 S	7.15.91.603	Radius	No	Up-scaled	Least Certain	Partial radius, only proximal end present. Scaled on maximum width.
MOR 553 S	7.28.92.105	Semilunate Carpal	Yes	Up-scaled	Less Certain	Scaled to match metacarpus. Immature element, unfused distal carpal 4.
MOR 553 S	8.20.92.303	Metacarpal I	Yes	Down-scaled	Less Certain	
MOR 553 S	8.13.92.237	Metacarpal II	No	Up-scaled	Less Certain	
MOR 553 S	7.16.92.1	Metacarpal III	No	Down-scaled	Less Certain	
MOR 553 L	7.25.9.312	Phalanx I-1	No	Up-scaled	Less Certain	Distal end spliced onto 563
MOR 563		Phalanx I-1	Yes	Up-scaled	Less Certain	Proximal end spliced onto 7.25.9.312.
MOR 553 S	2021-c-184	Phalanx I-2	No	N/A	N/A	
MOR 553 S	8.8.92.188	Phalanx II-1	No	Down-scaled	Least Certain	
MOR 553 S	7.22.92.58	Phalanx II-2	No	Up-scaled	More Certain	
MOR 553 S	7.9.9.172	Phalanx II-3	No	N/A	N/A	
MOR 553 L	7.24.88	Phalanx III-2	No	Up-scaled	Least Certain	
MOR 553 S	6.17.9.6	Phalanx III-4	No	N/A	N/A	
*Specimens scaled from greatest length of element unless specified otherwise. Certaintity based on complexity of scaling method. See materials for details.						

Scaling

Scaling was performed with the help of forelimb bone measurement tables (David Varricchio personal communication, February 22, 2022) that detailed the greatest lengths, widths, and other pertinent measurements for the *Troodon* forelimb elements held at the MOR. All fossil specimens used from MOR 553 were assumed to be from different individuals (Table 1), however forelimb elements preserved from MOR 563, were determined to be from a single associated individual. The greatest length recorded in the forelimb tables for each available specimen from MOR 563 was divided by the greatest length of a complete left humerus from MOR 563. This resulted in a scaling proportion for the applicable forelimb specimens, representative of the size difference of the element length relative to the humerus length. The scaled size for the specimens was calculated by multiplying the scaling proportion by the greatest length of a mature humerus from MOR 553, resulting in a maximum adult length for each appropriate specimen. This humerus (specimen number MOR 553 S, 8.2.92.303, Table 1) was selected for its overall condition and size, being identified as the most mature humeri preserved, and the only mature humeri that preserved the deltopectoral crest (David Varricchio personal communication, February 22, 2022).

Depending on element condition greatest length wasn't always possible, as some specimens were partial, so specialized approaches were needed. The scapula had to be scaled based on its maximum distal width instead of greatest length, as both MOR 553 and 563 scapula specimens were partial in length. This scaling factor was then multiplied by MOR 553's greatest humeral distal width, to approximate the scapula greatest width. This is the only element that was scaled based on the humerus greatest distal width and was decided based on the lack of greatest length information, and the completeness of both the humeral and scapula distal widths.

Both radii from MOR 553 and 563 were partial, and MOR 563 only preserves a section of the shaft, so the greatest shaft width was used to create a scaling factor. Because the distal section of the radii were unavailable, the radius scaling factor was multiplied by the humerus greatest length, to remain consistent with the rest of the specimens. Each of the metacarpals from MOR 563 were partial, so again the greatest length could not be used. However, the MOR 553 metacarpal specimens all preserved the complete length. For these specimens a scaling factor was first made comparing the greatest widths of each respective metacarpal from MOR 563 and 553. This factor was then multiplied by the greatest length of the MOR 553 metacarpal specimens, creating an estimate for the 563 metacarpal greatest lengths. This value was then used with the humerus greatest length scaling factor, resulting in another estimate based on the previously described humeral greatest lengths. Other elements, like the coracoid and unguals, weren't scaled using the above methods, and instead were scaled to match other paired elements.

The certainty of scaling factors used for each element is described in Table 1 and divides each scaling approach into three levels: More Certain, Less Certain and Least Certain. More certain is reserved for elements that were scaled using complete element lengths, whether greatest length or greatest width (green). Less certain was used when elements had more complicated scaling schemes, or they were made up composite elements (yellow). Least certain was used for specimens that were scaled based on abraded elements and partial elements that had to be estimated (red). An exhaustive description of the scaling process for each element is described in the materials section.

Additional Modification

Once scaled there were a few elements that required additional digital modification. The original MOR 553 specimen for phalanx I-1 is an incomplete element that doesn't fully preserve the proximal facet. MOR 563 phalanx I-1 preserves the proximal facet, but the distal end was not. The two complete surfaces from MOR 553 and 563 for phalanx I-1 were scaled and then spliced together, creating a hybrid element. Additionally, the ulna was broken into two separate pieces, most of the distal shaft, and a small section of the proximal surface. Both pieces could be matched together and merged digitally, preserving the original length of the element without any loss of size. Finally, the distal condyle of the humerus had a partially preserved articular surface, so the more complete articular surface from MOR 553 was used to aid in the manual touchup of the articular surface area using Maya's mesh shaping tools.

As mentioned previously, the only partial bones in the reconstruction were the coracoid, radius, and ulna. The partial coracoid preserves its contribution to the glenoid fossa, so the shoulder joint was able to be analyzed. The partial radius and ulna both retained the proximal ends of each respective element, so the elbow joint could also be analyzed. Lacking both the distal radius and the radiale, addressing hypotheses regarding wrist movement and mobility was not feasible. Additionally, since phalanges III-1 and III-3 were not present, digit III could not be tested. For the specific modifications and changes to each digital specimen see the materials section below.

Joint Construction

The finalized digital reconstruction created in Maya is representative of a nearly complete scaled left adult forelimb, being the first of its kind made for *Troodon*. Once finalized, each

digital bone was printed using a Formlabs Form 2 resin 3D printer at a 0.10 mm resolution, the same resolution with which the fossil bones were scanned (Formlabs, Somerville, MA). Once completed the 3D printed resin copies represent a 1:1 physical copy to the digital model. These physical counterparts to the digital reconstruction were used as a reference when designing and implementing the digital reconstruction. As the digital joint system was created, they were checked against the physical copies to confirm realistic joint movement and location.

From the completed digital reconstruction, a ROM assessment at each available joint could take place. This study opted for a traditional bone-on-bone ROM, where the spacing of soft tissues was ignored. This was done to help compare the study results with recently described troodontid material from Mongolia (Yu et al., 2022). In addition to measuring just flexion-extension (FE) angular movement this project also measured abduction-adduction (ABAD) and long axis rotation (LAR; Manafzadeh and Gatesy, 2021).

Shape Fitting Articular Surfaces . First, each finalized digital bone was individually imported from Maya into Geomagic Wrap 3D mesh software (Artec3D, Luxembourg). Once imported the articulated surfaces of each bone were manually highlighted (Figure 1, a). This was performed for the distal and proximal joint surfaces of each applicable bone, with the final highlighted joint surface saved as a separate digital mesh object in .Obj format. Due to bone and joint shape differences each bone required a slightly different approach to identify the joint surface. At its simplest this involved manually selecting the assumed articular surface (distal condyles and proximal facets). However, for some more complicated joints this required multiple iterations to create an expected joint axis (glenoid fossa).

Once the articular surface was identified and saved as a separate object an automated shape fitting algorithm in Geomagic was used on the saved shape to identify the joint central axis and center. This algorithm best fits a geometric primitive (Sphere, Cylinder or Plane) to the previously identified and saved joint shape (Figure 1, b). For this project, all joint surfaces studied were fit with cylinders. Using a cylinder treats each joint as a hinge-like joint, with the central axis of the cylinder used as the central axis and joint center (marked as the Z axis). The best fit algorithm can fit surprisingly different cylinders based on the initial shape provided, sometimes producing anatomically impossible joint axes. This proved to be the case even with articular surface shapes made from the same joint. As mentioned earlier, this meant that often the shape selection and shape fitting process had to be repeated multiple times to create a realistic and believable joint axis. Once an acceptable cylinder was created in Geomagic that shape was saved as both an .Obj file and as a Vrml1 file, that was used in the creation of a joint axis locator.

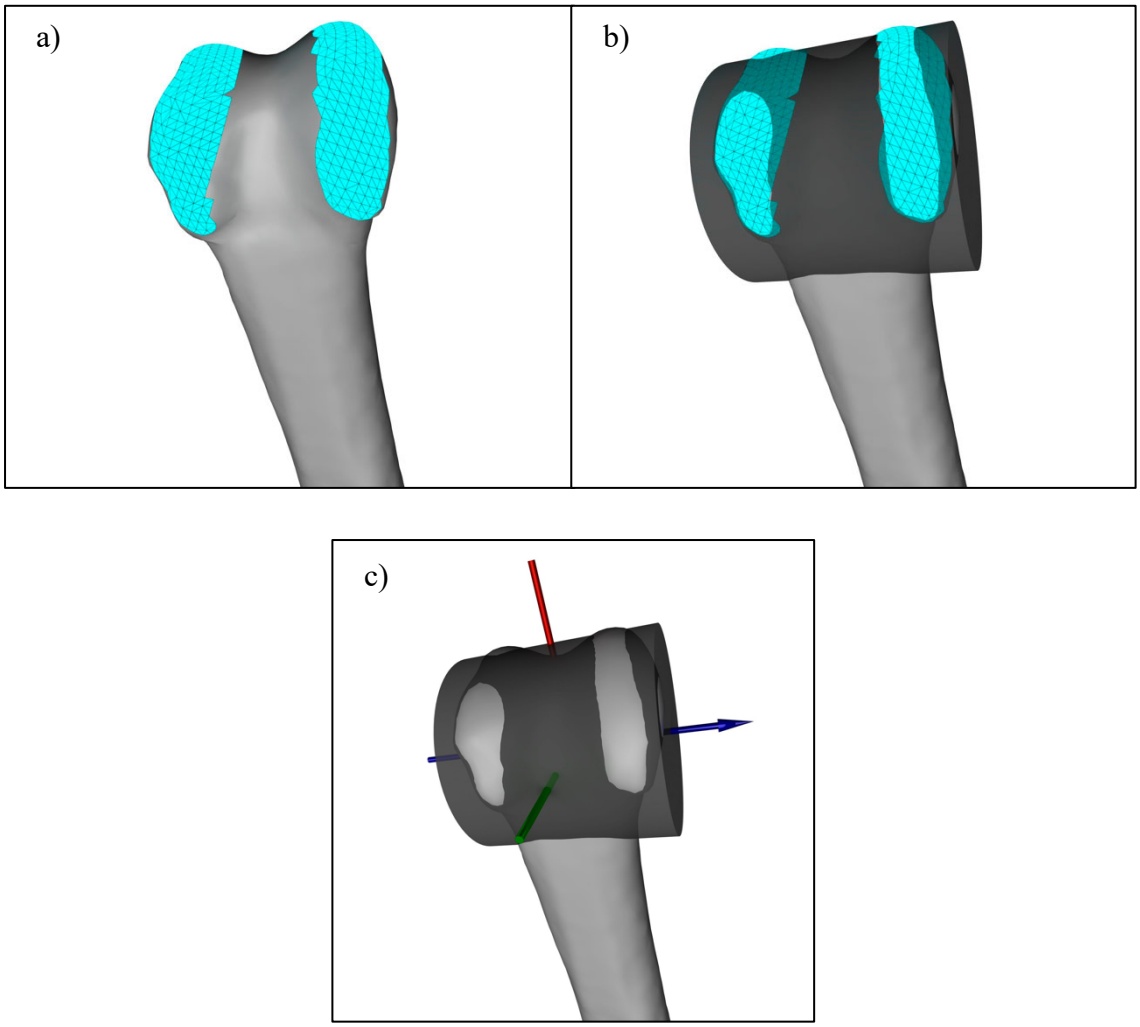

Figure 1: Step by step process for creating an anatomical coordinate system (ACS). a) Selection of articulated surfaces. b) Best fitting cylinders to selected shape. c) Creation of XYZ axes at cylinder center.

Creation of Joint Coordinate Systems (JCS's). Once the surface and cylinder were saved from Geomagic those shapes, along with the original bone mesh, were uploaded back into Maya. From Maya the joint shape and cylinders were imposed onto the bone itself, in the same position when created in Geomagic. This results in a series of cylinders at each joint surface, both proximal and distal, for each bone analyzed in the forelimb. Using custom code written for Maya (Gatesy et al., 2022), a set of XYZ mesh coordinates were fit to the center of each joint cylinder (Figure 1, c). When imported the Vrml1 file helped to create the Z axis at the center of the cylinder, representing the central axis of the joint's movement. The X axis was then re-oriented by hand, along the stationary Z axis, to point proximally following the length of the bone. The Y axis is representative of a floating axis and was not moved. This triple axis system was setup with the Z axis rotating in the direction of the bones flexion-extension axis (FE), the X axis matching long axis rotation (LAR), and the Y axis following abduction-adduction (ABAD). These axis systems are known as an anatomical coordinate system's (ACS's; Gatesy et al., 2010; Gatesy et al., 2021; Grood and Suntay, 1983).

Each joint is comprised of two ACS's, one on the proximal, or 'parent' bone and one on the distal or 'child' bone (Figure 2, a). Once in place, the child ACS for a given joint was oriented using the point and orient constraint function in Maya, so that it would lie directly on top of the parent ACS (Figure 2, b). This process lines up the X, Y and Z axes, putting both proximal and distal bone segments into alignment and forming a joint coordinate system (JCS; Gatesy et al., 2021; Bishop et al., 2021; Kambi et al., 2014;). In a JCS the proximal element serves as the 'parent' immobile element and the distal element serves as the 'child' mobile element that can be moved along the three primary axes.

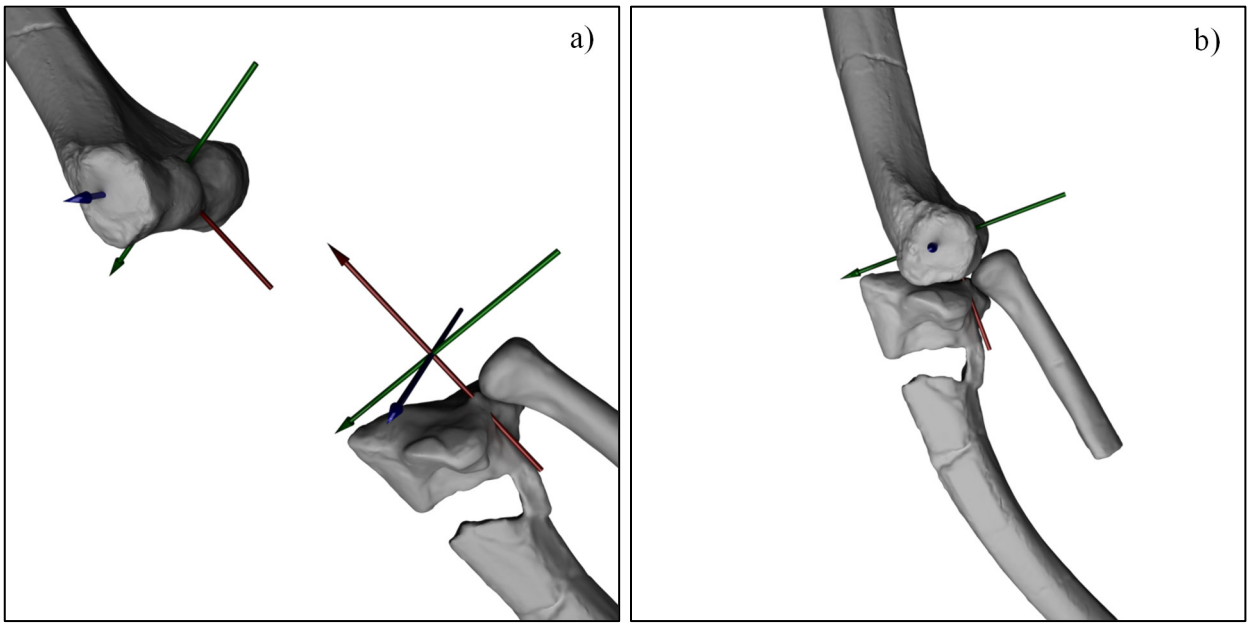

Figure 2: Process for linking two ACS's into a joint coordinate system (JCS). a) Two ACS's with XYZ axes oriented. b) Completed JCS with both ACS coordinates lying on top of each other.

Creating Joints at each JCS. Once linked into a JCS, 3D rigging joints in Maya were created and placed at each JCS center, matching the X, Y and Z axes of the joint to that of the JCS. This was performed using Maya's point and orient constraint tools, which exactly matches the point and orientation placement of the joint to the JCS. Joints in 3D rigging and animation are used to animate 3D models, rotating a section of a 3D model from a fixed point, not unlike a traditional armature in stop motion animation (Autodesk.com). Through a process called 'skinning' the joint was then locked to the 'child', or distal bone mesh. Once skinned, moving the joint would also move the bone that it was 'skinned' to. The exact movement of the joint, and by extension the JCS could then be measured in Euler degrees directly in the Maya software.

Zero Position Methodology

When initially setup each joint in Maya is placed in its 'zero position' where the Maya joint measures 'zero' degrees for each of the X, Y and Z axes. The placement of this position was determined by the initial location the X, Y and Z axes. Since the Z axes was largely predetermined by the fit cylinder shape, and the Y axes wasn't changed, the positioning of the X axis has the greatest effect. Different digital ROM studies have had different methodologies regarding the placement of the X axis, and by extension the zero position of each joint (Bishop et al., 2021; Gatesy et al., 2021). For this project the 'zero position' was selected by positioning the X axis down the long axis of each bone, pointing distally. When all the JCS's are linked together this results in the X axes linking into a straight line, with the long axis of each element parallel to one another and pointing distally (Figure 2). The option exists to mathematically determine the long axis using Matlab scripts, however for this project the long axis was picked by hand to save on time. This approach allowed for the quick acquisition of data and follows the starting position of other traditional ROM approaches (Senter and Sullivan, 2019; White et al., 2015; Yu et al., 2022).

Due to missing elements in the wrist, the *Troodon* forelimb was split into two separate JCS systems: the shoulder and elbow, and the manus with digits I-II. The only joints left out of this reconstruction were, digit III, and the wrist due to missing material. Even with the missing data, this reconstruction provides the first detailed evaluation of *Troodon* forelimb and manus range of motion.

Soft Tissue Estimation

The effects of soft tissue on joint function and ROM have made a large impact on the study of extinct species. Previous studies used phylogenetic bracketing techniques to determine ideal spacing to add for cartilage and other soft tissues in the hindlimbs within archosauria (Hutchinson et al., 2005). This spacing was applied to the forelimb joints in this study, however upon further inspection and comparison with other living species it was deemed too large. Further study into the specifics of forelimb cartilaginous spacing will be required before spacing can be standardized for use in biomechanical studies (Senter and Sullivan, 2019). Due to these complications, this study opted to orient the bones as close together as possible to simulate the 'bone on bone' approach and allows for the comparison with other similarly conducted studies (Senter and Sullivan, 2019; White et al., 2014; Yu et al., 2022). It's important to note that allowing for a reasonable range of motion without bone overlap required a minimal amount of spacing for certain joints. Each joint was manually manipulated to ensure that interpenetration of the bone through a standard rotation of the Z axis (FE) was avoided, but there is still likely to be some inconsistency as this was performed by hand.

Range of Motion (ROM) Measurement

Testing ROM in three axis (representative of three out of six degrees of freedom) instead of the traditional one poses additional complications for data collection. In the past tables detailing the separate measurements have been applied, as have animations showing the proposed movement (Manafzadeh and Gatesy, 2022). The latest studies use simulations to systematically measure joint movement and use Boolean processes to remove impossible orientations based on interpenetrating bone (Manafzadeh and Padian, 2018). This can be very

important in testing all six degrees of freedom, as small changes in one axis can have a large effect on another. Due to time constraints this study was unable to apply this latest methodology, instead opting for manual manipulation of each joint through its range of motion at each of the angular degrees of freedom.

Boolean Creation in Blender. To help with identifying interpenetration of bone the entire mesh and joint model was imported into Blender (Blender Foundation, Amsterdam) where Boolean modifiers were added to copies of each bone mesh, as inspired by previous studies (Manafzadeh and Padian, 2018; Manafzadeh and Gatesy, 2022). These copies occupied the same space as the original bone meshes but were programmed to create a bright pink Boolean mesh when the bone meshes intersected. This approach, while not automated, still allowed for precise, quick, and objective data collection. While using Boolean intersection operations are not new to ROM studies, their use in the Blender animation software in this way represents a novel approach.

Joint Measurement Characteristics. Using the Boolean modifiers, the edge of each movement was identified either as bone-on-bone contact (i.e. – Boolean creation), or the edge of the joint's articular surfaces as defined by Senter and Sullivan, 2019, whichever occurred first. While identifying Boolean creation was able to be performed objectively (either a pink shape was, or was not made), identifying the edge of each joint was more subjective. As defined by Senter and Sullivan, 2019: "To implement the bare-bones method of ROM estimation, the edges of the articular surfaces are identified as precisely as possible on the basis of abrupt changes in texture and/or topology, which are more obvious in some cases than in others.", making it an inherently subjective process from joint to joint.

Measurement Process. Each element was first measured in three orientations on the Z axis: maximum flexion, maximum extension and at rest (zero position). From these three orientations the angular range of motion along the X axis (representing long axis rotation) and the Y axis (representing abduction-adduction) were then independently measured. This is a simplified assessment of movement that excludes translational degrees of freedom but was necessitated due to the constraints of this current study. This approach was chosen to provide a good overview of potential movement, including not only flexion and extension but the previously mentioned abduction-adduction and long axis rotation.

Physical Measurement of 3D Printed Bones. Throughout this process the previously made 3D printed copies of the forelimb bones were used to help check the digital reconstruction results for selected joints. Using modeling clay to hold bones together the joint angles were measured with via protractor and results recorded to the closest whole degree. The physical copies have the added benefit of being easier to manipulate and don't interpenetrate like digital copies do. This made for quick reference and double checking of joints, especially when movements weren't as obvious on the digital model. The physical models were used to help confirm the ROM for all the manual joints in digits I and II but were less helpful with more complicated joints like the shoulder and elbow that had more than two bones interacting.

Materials

Scapula

The scapula and coracoid used for this study come from MOR 553 and are from two separate individuals (Table 1). The scapula features a long thin blade which curves medially. This curve is representative of the living position of the scapula and shows no signs of crushing or taphonomic alteration, presumably following the curve of the ribcage. The distal most extremity of the scapular blade is broken, so true total length is unknown. The distal section of the scapula, however, is in one piece preserving the glenoid fossa, acromial process, and coracoid suture.

Since the scapulae for both MOR 553 and 563 didn't preserve the greatest length, the scaling was based on their greatest width instead. This was measured as the distance between the most anterodorsal point of the acromial process and the most posterodorsal section of the glenoid fossa, which was preserved in both MOR 553 and 563. This greatest width measurement from MOR 563 was divided by the greatest distal width of the humerus from MOR 563, defined as the maximum width across the humeral distal condyles. Dividing both measurements created a proportion of the scapula width by the humerus width. This proportion was multiplied by the humerus distal width from MOR 553, providing a distal width estimate that was used to scale the MOR 553 scapula in Maya up 1.618 times its original size. The humerus distal width was chosen to scale the scapula, instead of the greatest humeral length, due to the incomplete scapular lengths from both MOR 553 and 563. Considering the element completion for the distal widths of both the scapulae and humeri, the scaling for this specimen is more certain (Table 1). Once scaled, the scapula was mirrored to match the left side material.

Coracoid

The coracoid from MOR 553 is a bulky irregular piece of bone, with the medial most portions of the bone having been lost. The resulting preserved portion of the coracoid includes the entirety of the glenoid fossa and portions of the anterior and posterior margins. The dorsal portion of the acromial process appears to be lost or worn down. The entirety of the suture to the scapula, however, is preserved featuring an elongate ovoid shape that is slightly concave with an irregular bumpy surface. Due to the completeness of the glenoid surface on both the coracoid and scapula the complete glenoid fossa is present in its entirety, allowing for the analysis and reconstruction of the shoulder joint.

Since the suture surface connecting the scapula and coracoid were preserved in both MOR 553 specimens, this allowed for a convenient landmark to scale the coracoid to. Using the size of the suture surface from the scaled scapula the suture surface of the coracoid was scaled in Maya to match, increasing the coracoid 1.046 times its original size, as measured from its greatest length. Once scaled in this fashion the glenoid surfaces of both the scapula and coracoid were examined and determined to be of equal width. Considering that the coracoid was scaled to match the scapula the scaling for the coracoid is considered more certain (Table 1). The coracoid was also mirrored to match the left side material.

Humerus

The humerus used in this reconstruction is based on two bones from MOR 553, 92-303 and 0-96 (Table 1). Both humeri are robust and stocky, identified as mature elements (David Varricchio, personal communication, February 22nd, 2022). Considering the maturity of the humeri, specifically 92-303, the humerus is one of four bones in the reconstruction that were not

scaled, which also includes the three unguals, making the digital version a 1:1 copy of the physical specimen.

The deltopectoral crest (DPC) preserved in 92-303 is present almost in its entirety. All the other mature humeri preserved from Jack's Birthday Site, including 0-96, have DPC's that are fractured or damaged. In 92-303 there is only a small hole in one portion of the DPC, but it preserves the entirety of its length. The DPC is relatively long, covering almost half the total length of the humerus in *Troodon*. The distal condyles preserved in 92-303 are the only part that was found to be partial, lacking the definition present in other similarly sized humeri from MOR 553. To address this the condyles in the digital copy of 92-303 were manually modified. Using the more complete condyles from 0-96 as a guide, and the mesh modeling tools in Maya, the condyles in 92-303 were shaped to better match a more complete set. The final version of the humerus is a composite. It's important to note that the modifications made do not alter the greatest length, or greatest width of 92-303, outside of the condyles the rest is original to 92-303.

Ulna

The ulna is nearly complete but had the proximal articular surface broken off the rest of the shaft. Despite being broken there was enough of the bone remaining to match the anterior and posterior portions of the bone together without any apparent loss of length or taphonomic alteration. The digital copies of the distal and proximal pieces were combined in Maya into a single digital object, reflecting the ulna's original length.

Once re-assembled the ulna was scaled using the greatest humeral lengths from MOR 553 and 563. The greatest length recorded for the ulna from MOR 563 was divided by the greatest humeral length from MOR 563, creating a scaling proportion. This proportion was

multiplied by the greatest length of the MOR 553 humerus, providing the estimated length for the 553 ulna, which was digitally scaled to 1.246 times its original size in Maya. Even though it was broken, the re-assembled greatest length of the MOR 553 ulna, along with the length from MOR 563, were in good condition. As such the scaling for this specimen is more certain (Table 1).

Radius

Both radii from MOR 553 and 563 are partially preserved. The radius from MOR 553 preserves the proximal most section of the bone including the proximal articular surface and a short section of the shaft. The proximal surface is complete and in good condition, as is the shaft until it is cut off perpendicular across the shaft. The radius from MOR 563 preserves only the central section of the shaft. The bone surface on MOR 563 is rough and shows signs of abrasion.

Considering the partial nature of both radii the scaling process used the greatest shaft width, instead of length or distal width. The greatest width from the MOR 563 radius was divided by the greatest humeral length from MOR 563, creating a scaling proportion. This scaling proportion was multiplied by the MOR 553 humeral length, providing an estimate for the 553 radius width, which was scaled in Maya 1.427 times its original size. Since the distal width was not available for both radii it was decided to stick to the humeral length as a scaling factor to remain consistent with the rest of the forelimb elements. Considering the condition of the MOR 563 and 553 radius specimens this specimen is considered least certain (Table 1).

Semilunate Carpal

The majority of the semilunate carpal from MOR 553 is complete and in good condition, clearly showing the proximal and distal articular surfaces in fine detail. The semi-circular shape

indicative of its name is clearly visible from the lateral side of the bone and bears a weak concavity. The medial side by contrast is oblong to sub-rounded in shape and deeply concave. The distal articular surfaces fit very snuggly with metacarpals I and II. Almost all the proximal condyle for metacarpal II connects with this surface, while only a portion of metacarpal I connects. The proximal articular surface is saddled and convex lengthwise, but slightly concave along its width, as is typical for other members of Paraves. At the medio-ventral corner there is a small convex facet. Based on comparison with similar taxon this is representative of an unfused distal carpal 4, indicative of an immature individual and the relative incompleteness of the carpal (Xu et al., 2014). Based on this, the semilunate carpal is likely representative of the most juvenile element used in this reconstruction.

Due to a lack of semilunate carpals preserved for MOR 563, and the good condition of the distal articular surface in MOR 553 this specimen was scaled to visually fit the proximal condyle for metacarpals I and II. To achieve this the semilunate carpal was scaled in Maya up 1.548 times its original size. This resulted in a good visual, and physical fit, with the digital and printed copies confirming a good fit between the metacarpals and the semilunate. Since the scaling for the semilunate is based largely off the scaling of the other metacarpals, especially metacarpal-II, its scaling certainty is less certain (Table 1).

Metacarpal-I

Metacarpal-I is the smallest of the three metacarpals, as is typical of most theropods. The MOR 553 specimen features a short shaft, triangular in cross section, that connects to an asymmetrical distal condyle at an angle, with the condyle pointed antero-dorsally. The condyle itself has a ginglymoid articular surface, with the ventral surface larger than the dorsal. The

ventral condyle is curved when viewed anteriorly. The flat ventral side of the bone fits very snugly next to metacarpal-II, with the curve of the ventral condyle of metacarpal-I also fitting closely into the curved shaft of metacarpal-II.

Metacarpal-I, like the other metacarpals from MOR 563, don't preserve the greatest length of the element, so two scaling proportions were used. First, the greatest proximal width between MOR 563 and 553 were divided, creating a scaling proportion between the two metacarpals. This proportion was multiplied by the greatest length of the MOR 553 metacarpal I, creating an estimate for the greatest length for the MOR 563 metacarpal-I. This greatest length was then divided by the greatest length from the MOR 563 humerus, creating a second scaling proportion. This final proportion was multiplied by the greatest length from MOR 553's humerus, resulting in a length for the MOR 553 metacarpal-I. Once fully scaled metacarpal-I is one of the few specimens, other than metacarpal-III and phalanx II-1, that were scaled down, having been scaled down in Maya 1.009 times its original size. Considering the complicated process required to scale metacarpal-I, the scaling certainty is defined as less certain (Table 1).

Metacarpal-II

Metacarpal-II is the longest and largest of the three, again as is typical for most members of Paraves. The MOR 553 specimen is in excellent condition, showing no evidence of breakage or abrasion. The proximal condyle is triangular when viewed proximally, with a rounded, smooth surface that curves dorsolaterally. There are two flattened sections of the proximal shaft that contribute to its triangular shape, one faces antero-medially, while the other faces postero-medially. These facets fit the other metacarpals well, with the anterior facet fitting metacarpal-I

and the posterior facet fitting metacarpal-III. With all 3 metacarpals in place the metacarpus has a distinctly sub-circular outline when viewed proximally.

Like metacarpal-I, metacarpal-II was also scaled using two scaling proportions. The first proportion was collected by dividing the distal widths of metacarpal-II from both MOR 563 and 553. That proportion was then multiplied by the greatest length from the MOR 553 metacarpal-II specimen, resulting in an estimated MOR 563 metacarpal-II greatest length. This greatest length was then divided by the MOR 563 humeral greatest length, creating a second proportion. Multiplying this proportion by the MOR 553 humeral length provided the MOR 553 metacarpal-II length, which was increased in Maya 1.402 times from its original size. Since metacarpal-II followed a similar scaling process as metacarpal-I, both have been defined as less certain (Table 1).

Metacarpal-III

The MOR 553 metacarpal-III is a long thin bone preserved in good detail. Metacarpal-III has a proximal condyle roughly triangular in cross section when viewed proximally. This triangular condyle forms a wedge that tapers away from the rest of the metacarpus and is opposite the face that connects with metacarpal-II. When viewed dorsally the proximal head of metacarpal-III angles medially, toward metacarpal-II.

Following the other two metacarpals, two scaling proportions were used to reach a greatest length estimate for metacarpal-III. Following the process used for Metacarpal-II, the distal widths from the MOR 563 and MOR 553 metacarpal-III specimens were used to create the first proportion. This proportion was multiplied by the greatest length from the MOR 553 metacarpal-III, giving an estimate for greatest length for the MOR 563 metacarpal-III. This

greatest length was divided by the humeral greatest length from MOR 563, creating the second proportion. Finally, this proportion was multiplied by the MOR 553 humeral greatest length, providing the estimate for the MOR 553 metacarpal-III length. Metacarpal-III is only one of three specimens, including metacarpal-I and phalanx II-1, that were downscaled being decreased in Maya 1.0003 times its original size. Following the other two metacarpal scaling certainties, metacarpal-III is being defined as less certain (Table 1).

Phalanx I-1

Phalanx I-1 is a composite element made by splicing the proximal half of I-1 from MOR 563 with the distal half of I-1 from MOR 553 (Table 1). This was done because the proximal facet in MOR 553 was partial but was complete in MOR 563.

First each specimen was scaled by dividing the greatest length of phalanx I-1 from MOR 563 by the greatest humeral length from MOR 563, creating a scaling proportion. This proportion was multiplied by the greatest humeral length from MOR 553, creating an estimated total length for phalanx I-1. This length was used for both MOR 553 and 563 phalanx specimens. Once scaled, phalanx I-1 from MOR 563 was mirrored to match MOR 563. Next, the proximal section of phalanx I-1 from both MOR 563 and 553 were spliced off at the same length down the shaft. The proximal section from MOR 563 was then attached to the distal section of MOR 553, creating one composite phalanx. Total length and width were preserved as best as possible, ultimately approximating a complete phalange. Phalanx I-1 from MOR 553 was increased in size 1.652 times its original size and MOR 563 was increased by 1.672 times. Due to the composite nature of the element, the scaling for phalanx I-1 is being defined as less certain (Table 1).

Ungual Phalanx I-2

The first ungual phalanx is the largest and most developed, typical of other theropods. It is thickest at its most proximal, curving and thinning as it transitions distally showing a strongly recurved shape. When viewed proximally the proximal condyle can be seen as an oblong facet of bone, roughly divided into unequal concave troughs by a raised convex ridge in the middle. Just ventral to the proximal condyle the flexor tubercle is rounded and well developed. The ungual is quite thin in profile, showing a weak taper as it transitions distally, with the distal most tip broken off. Ungual I-2, like all the other unguals and the humerus, were not scaled. It was determined that scaling was not necessary based on the fit that each ungual had with their respective phalanges. This was checked with both the digital and physical copies of the bone, confirming an appropriate fit.

Creating the joint coordinate system (JCS) for the first ungual wasn't as straightforward as detailed in the methods. The proximal condyle of ungual I-2 is asymmetrical, so the shape fitting algorithm had difficulty creating a joint axis that followed the direction of the joint movement. To remedy this the Z axis was manually moved to better reflect realistic joint movement. While this changed the direction of the joint axis, the center of the joint as picked by the shape fitting algorithm was not changed.

Phalanx II-1

The first phalanx on the second digit is in good condition, and except for minor crushing on the dorsal facing section of the shaft, it's a complete and unaltered bone. Proximally there are two facets of unequal size, a smaller dorsal and larger ventral facet. The proximal facets fit snuggly with the distal condyle from metacarpal II.

Phalanx II-1 was scaled by dividing the greatest length from the MOR 563 II-1 specimen with the humeral greatest length from MOR 563, creating a scaling proportion. This proportion was multiplied by the greatest humeral length of MOR 553, creating an estimated total length for MOR 553 phalanx II-1. Of important note, the MOR 563 phalanx II-1 specimen was partial in length, and its total length was estimated, so the size determined may be off. Since its based off an incomplete element phalanx II-1's scaling certainty is least certain (Table 1).

The MOR 553 specimen is one of three specimens that were decreased in size, the other two being metacarpals I and III. Phalanx II-1 was decreased 1.034 times its original size.

Phalanx II-2

The second phalanx of the second digit is the longest of the phalanx bones. The shaft for the MOR 553 specimen was broken in two places, and as such is not perfectly straight. Aside from the breakage II-2 is in good condition and shows clear joint surface detail.

Phalanx II-2 was again scaled using the greatest length of the MOR 563 II-2 phalanx divided by the MOR 563 humeral greatest length and multiplying that result by the greatest length of the MOR 553 humerus. This final measurement was used to increase the MOR 553 phalanx II-2 1.373 times its original size. Considering the relative completion of the elements used, the scaling certainty for phalanx II-2 is defined as more certain (Table 1).

Ungual Phalanx II-3

The second ungual is noticeably dorsoventrally smaller compared to the first. Proximally the ungual has a similarly shaped, albeit smaller, proximal condyle that shares the same convex ridge and concave troughs. In comparison to ungual I-2 the proximal condyle for II-3 is dorsoventrally shortened and mediolaterally expanded. The flexor tubercle is still rounded but

has much less relief when compared to I-2. When viewed laterally II-3 has a faintly teardrop shape, tapering to a fine point. Like the other unguals, phalanx II-3 was not scaled (Table 1). unlike ungual I-2, II-3 did not need adjustment to its JCS.

Phalanx III-2

Phalanx III-2 is the only complete phalanx preserved for digit III. Like other theropods it is much shorter than other phalanges and features a very prominent proximal facet. The proximal facet features pronounced extensions on the dorsal and ventral sides that extend proximally, forming a rounded extension presumably to contact with phalanx III-1. The short shaft is rounded dorsally and flat ventrally, quickly transitioning to a rectangular cross section at the distal condyles. The distal condyles are nearly equal in size and shape, and taper as they transition from the ventral to dorsal surface of the phalanx.

Phalanx III-2 was again scaled by dividing the MOR 563 phalanx III-2 greatest length by the MOR 563 humeral greatest length and multiplying the resulting proportion by the humeral length of MOR 553. When applied in Maya this resulted in increasing the phalanx 1.275 times its original size. Importantly, the MOR 563 phalanx III-2 was partial, and its total length estimated, so the estimated value of the MOR 553 phalanx may be off. Based on the partial length of the scaled element the scaling certainty is least certain (Table 1).

Ungual Phalanx III-4

The last ungual phalanx is the smallest of the three and is also the most partial. The distal most end of the ungual is broken, and the flexor tubercle is completely missing. The general dorsal curvature is visible, as is the dorsal portion of the proximal facet. Like the other unguals, ungual phalanx III-4 wasn’t scaled.

RESULTS

Joint Range of Motion

In total, the range of motion (ROM) for seven joints for *Troodon* were analyzed for this study. Joints analyzed include the shoulder, (scapula-coracoid and humerus) elbow, (humerus and ulna-radius) and all phalangeal joints from digits I and II, including the ungual joints. All joints were measured from three degrees of freedom, represented by the X, Y and Z axes of the JCS's. Movement along the Z axis represents flexion and extension (FE) and was recorded from three frames of reference: maximum flexion (Figure 5: a, b), maximum extension (Figure 5: c, d) and the zero pose (Figure 5: e, f). From each FE reference position, the maximum angular values for the other two axes were measured, abduction and adduction (ABAD), represented by the Y axis, and long axis rotation (LAR), represented by the X axis (Manafzadeh and Gatesy, 2021). ABAD and LAR were independently measured for each of the FE reference frames. Consistent with findings from other dromaeosaurid and troodontid manual ROM studies (Senter & Parrish, 2005; Senter, 2006; Yu et al., 2022), almost all the forelimb joints analyzed for *Troodon* had higher ranges of flexion than extension. ROM results for each joint are presented in detail in Table 2. Joints of interest and general patterns are discussed below.

Shoulder

The shoulder was found to have a total measured ROM of 167 degrees. Both flexion and extension were nearly equal, with the flexion angle higher by ~5 degrees than extension, being the only joint with such a close margin (Figure 3). Abduction and adduction ROM for all three reference positions averaged 29.67 degrees. Long axis rotation across all three positions

averaged 31.30, however there were certain poses where maximum LAR appeared to dislocate the humerus from the glenoid, so is unlikely to reflect realistic in vivo mobility.

Antebrachium

The elbows maximum FE ROM was measured at 141.59 degrees, with significantly higher flexion than extension (Figure 4, a). ABAD and LAR increased as the flexion angle increased. This assumes, however, that the radius was flexible relative to its position with the ulna. If this assumption is incorrect, then the radius would contact the humeral shaft at a much lower ABAD and LAR angles under maximum flexion.

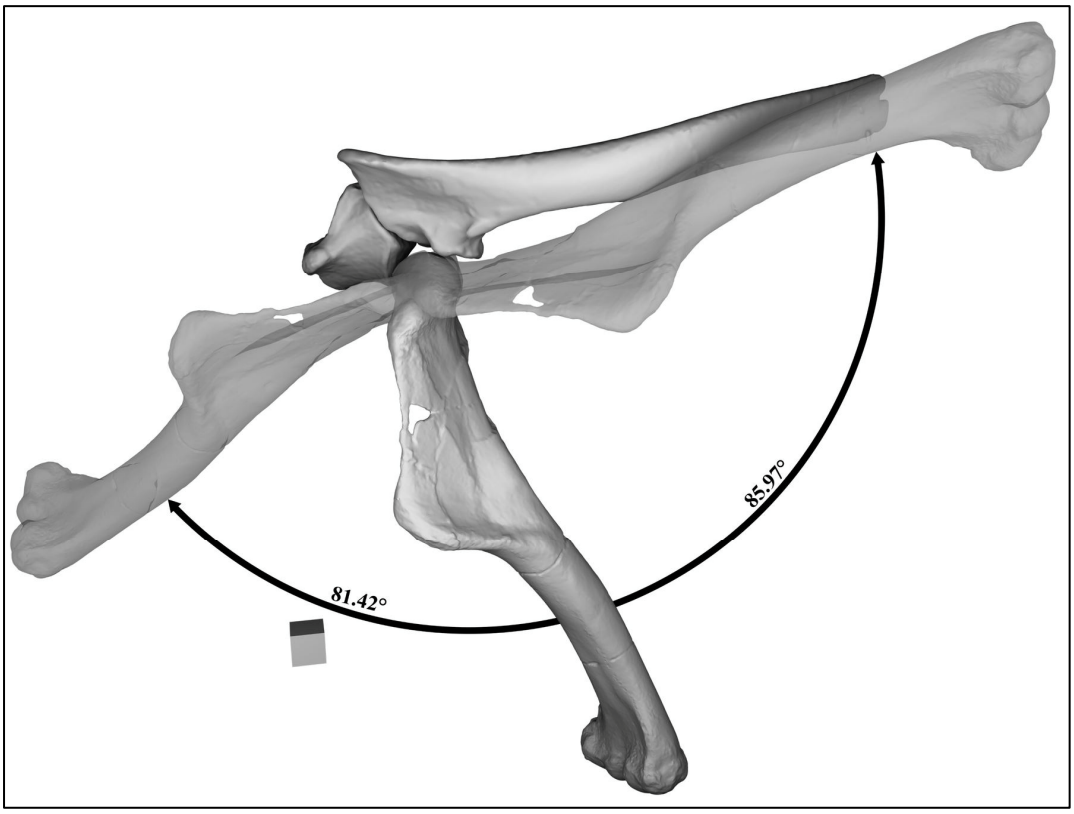

Figure 3: Flexion extension (FE) range of motion for the *Troodon* shoulder. Scale cube is 1cm.

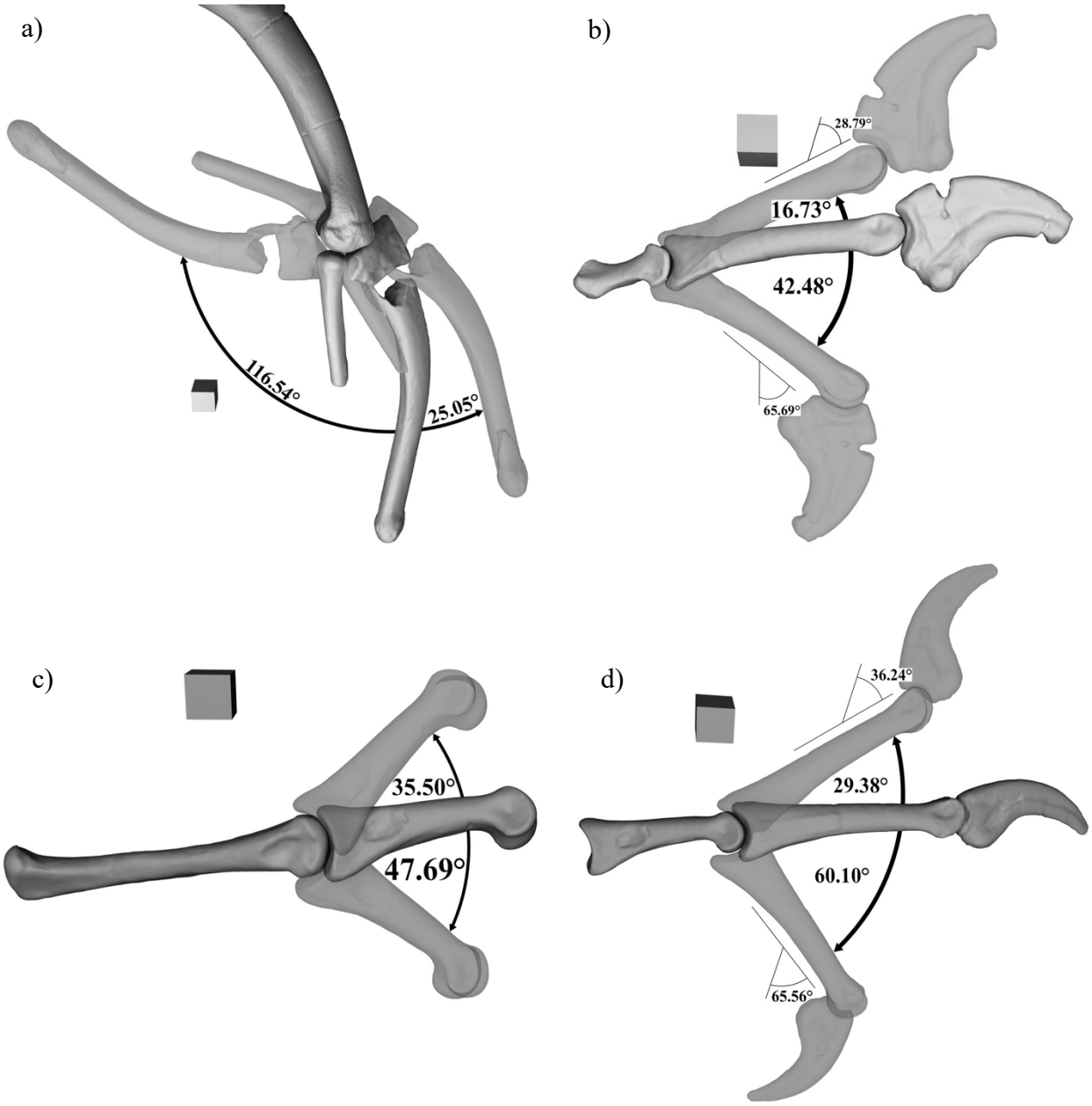

Figure 4: FE range of motion for the a) Elbow, b) Digit I, c) Phalanx II-1, d) Phalanges II-2 and II-3. Scale cube is 1 cm.

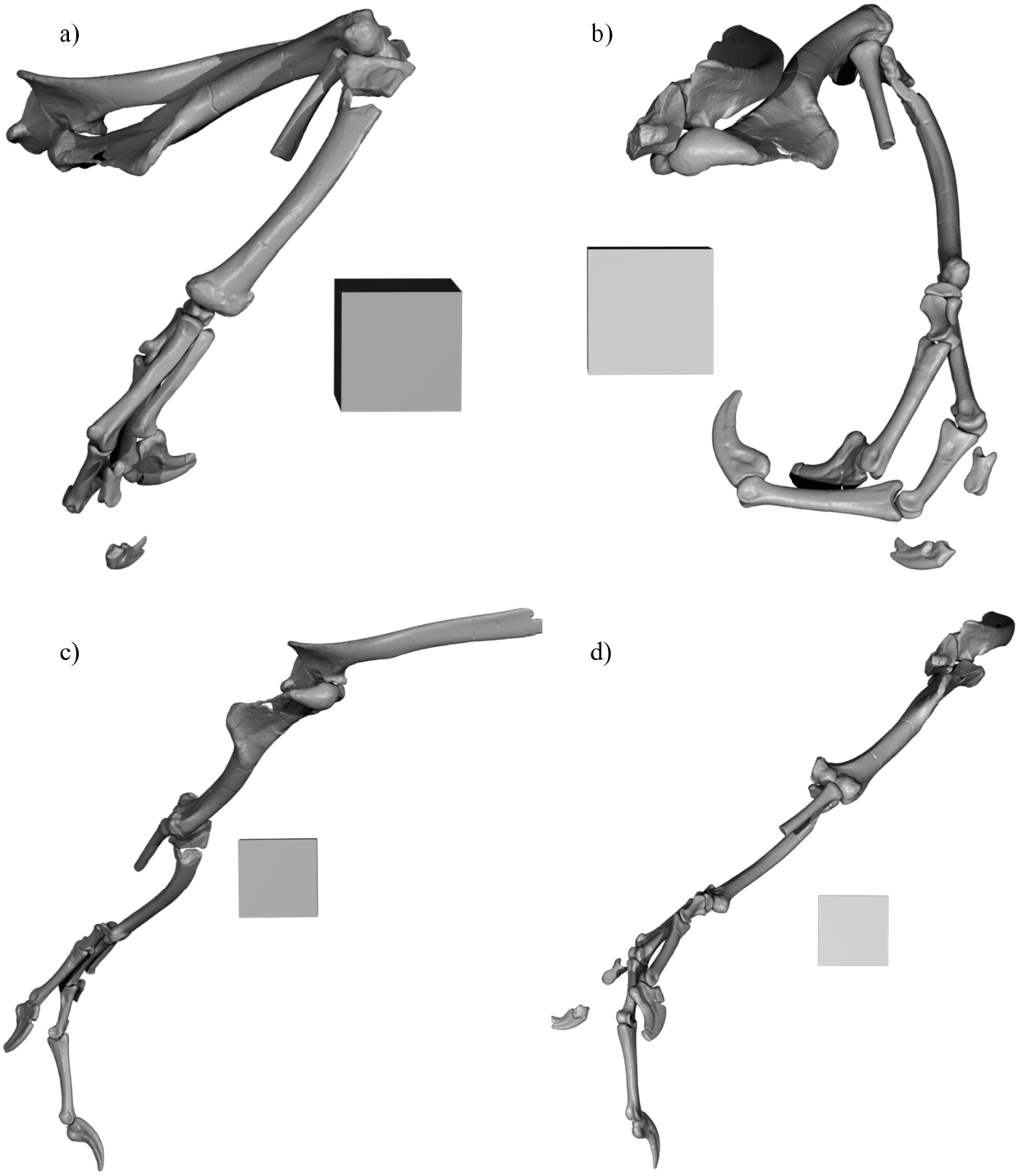

Figure 5: Lateral (a, c, e) and anterior (b, d, f) views of the *Troodon* forelimb at flexion (a, b) extension (c, d) and zero (e, f) positions. Scale cube is 5 cm.

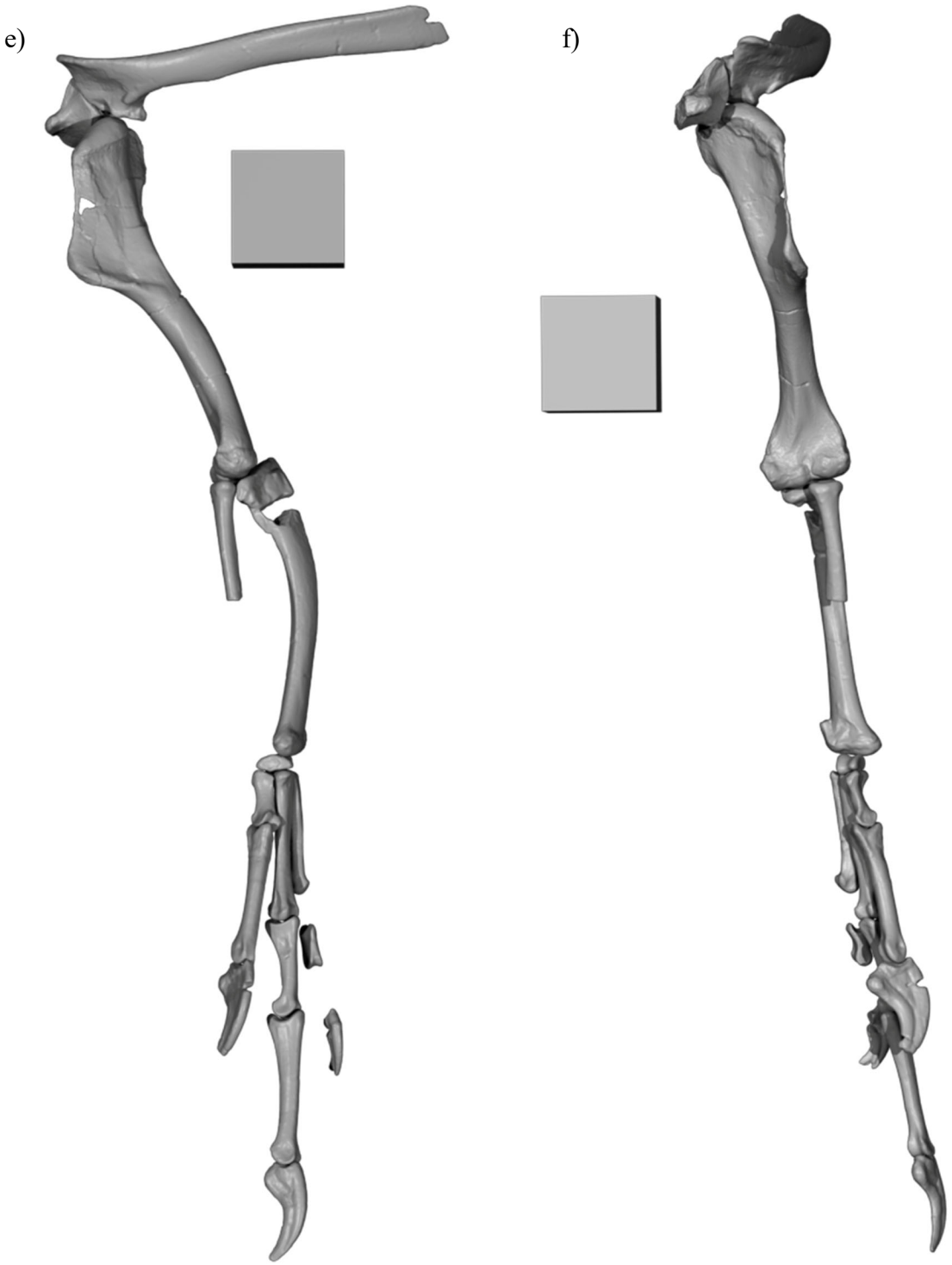

Figure 5 Continued: Lateral (a, c, e) and anterior (b, d, f) views of the *Troodon* forelimb at flexion (a, b) extension (c, d) and zero (e, f) positions. Scale cube is 5 cm.

Table 2: *Troodon* Forelimb ROM Measurements in Euler Degrees

***Troodon* Left Forelimb ROM Table (Euler-Degrees)**						
Joint	**Flexion-Extension Z (FE)**		**Abduction-Adduction Y (ABAD)**		**Long axis Rotation X (LAR)**	
Shoulder	E	81.42	AB	(0.02) 10.27	Sinistral (L)	0.00
			AD	23.84	Dextral (R)	17.57
			Total ROM	**34.11**	**Total ROM**	**17.57**
	Mid (zero)	0	AB	15.33	Sinistral (L)	12.28
			AD	18.58	Dextral (R)	13.32
			Total ROM	**33.91**	**Total ROM**	**25.60**
	F	85.97 (55.87)	AB	20.99	Sinistral (L)	0.00
			AD	0.00	Dextral (R)	"-50.72"
	Total ROM	**167.39**	**Total ROM**	**20.99**	**Total ROM**	**50.72**
Elbow	E	25.05	AB	2.92	Sinistral (L)	0.00
			AD	0.01	Dextral (R)	6.45
			Total ROM	**2.93**	**Total ROM**	**6.45**
	Mid (zero)	0	AB	5.75	Sinistral (L)	10.98
			AD	8.38	Dextral (R)	18.96
			Total ROM	**14.13**	**Total ROM**	**29.94**
	F	116.54	AB	(0.00) 9.04	Sinistral (L)	9.79
			AD	(4.50) 10.21	Dextral (R)	(0.03) 31.02
	Total ROM	**141.59**	**Total ROM**	**19.25**	**Total ROM**	**40.81**
Phalanx I-1	E	(16.73) ~25.00~	AB	0	Sinistral (L)	6.69
			AD	16.49	Dextral (R)	0.00
			Total ROM	**16.49**	**Total ROM**	**6.69**
	Mid (zero)	0	AB	(2.16) ~26.00~	Sinistral (L)	6.37
			AD	12.99	Dextral (R)	4.76
			Total ROM	**38.99**	**Total ROM**	**11.13**
	F	42.48	AB	0.00	Sinistral (L)	0.00
			AD	15.32	Dextral (R)	20.68
	Total ROM	**59.21**	**Total ROM**	**15.32**	**Total ROM**	**20.68**
Ungual Phalanx I-2	E	"84.19" 28.79	AB	6.34	Sinistral (L)	20.09
			AD	2.84	Dextral (R)	12.69
			Total ROM	**9.18**	**Total ROM**	**32.78**
	Mid (zero)	0	AB	12.52	Sinistral (L)	8.39
			AD	4.05	Dextral (R)	25.96
			Total ROM	**16.57**	**Total ROM**	**34.35**
	F	"83.99" 65.69	AB	27.49	Sinistral (L)	"29.07"
			AD	9.66	Dextral (R)	"13.38"
	Total ROM	**94.48**	**Total ROM**	**37.15**	**Total ROM**	**42.45**
"Values are likely unrealisticaly high, appear to dislocate joint"						
~Values measured from physical specimens~						
(Values were prematurely interpenetrated by mesh, reflect unrealistically low ROM)						

Table 2 Continued: *Troodon* Forelimb ROM Measurements in Euler Degrees

Phalanx II-1	E	"88.94" 35.50	AB	5.41	Sinistral (L)	18.61
			AD	15.15	Dextral (R)	20.86
			Total ROM	**20.56**	**Total ROM**	**39.47**
	Mid (zero)	0	AB	7.59	Sinistral (L)	15.25
			AD	10.44	Dextral (R)	16.39
			Total ROM	**18.03**	**Total ROM**	**31.64**
	F	"85.99'" 47.69	AB	5.89	Sinistral (L)	15.77
			AD	1.57	Dextral (R)	12.95
	Total ROM	**83.19**	**Total ROM**	**7.46**	**Total ROM**	**28.72**
Phalanx II-2	E	"65.28" 29.38	AB	12.85	Sinistral (L)	2.16
			AD	1.70	Dextral (R)	14.82
			Total ROM	**14.55**	**Total ROM**	**16.98**
	Mid (zero)	0	AB	15.71	Sinistral (L)	14.64
			AD	16.57	Dextral (R)	20.71
			Total ROM	**32.28**	**Total ROM**	**35.35**
	F	"108.60" 60.10	AB	6.40	Sinistral (L)	28.51
			AD	24.65	Dextral (R)	7.11
	Total ROM	**89.48**	**Total ROM**	**31.05**	**Total ROM**	**35.62**
Ungual Phalanx II-3	E	"52.54" 36.24	AB	7.20	Sinistral (L)	15.50
			AD	7.53	Dextral (R)	12.51
			Total ROM	**14.73**	**Total ROM**	**28.01**
	Mid (zero)	0	AB	3.05	Sinistral (L)	12.40
			AD	9.03	Dextral (R)	4.76
			Total ROM	**12.08**	**Total ROM**	**17.16**
	F	65.56	AB	0.00	Sinistral (L)	0.00
			AD	1.16	Dextral (R)	1.47
	Total ROM	**101.8**	**Total ROM**	**1.16**	**Total ROM**	**1.47**

"Values are likely unrealisticaly high, appear to dislocate joint"
~Values measured from physical specimens~
(Values were prematurely interpenetrated by mesh, reflect unrealistically low ROM)

Phalanges

The phalangeal joints follow a similar set of patterns in their ROM, and so will be discussed together here (Figure 4: b,c,d). Every phalangeal joint had its maximum flexion and extension angle determined by the overlap of the proximal and distal articular surfaces. Bone on

bone contact was deemed too excessive a measure, as it appeared to dislocate the joints in most cases (Figure 6). The maximum bone on bone contact angles were still recorded in Table 2 but were not used for ROM estimates or hypothesis testing. Consistent with prior ROM studies for dromaeosaurs and troodontids the range of flexion was higher than extension for all phalangeal joints analyzed (Figure 8). However, both ungual joints showed consistently higher ROM than the other phalangeal joints, with an average FE ROM of 98.14 for ungual joints and 77.29 degrees for phalangeal joints. The maximum allowed adduction for phalanx I-1 was interrupted by metacarpal II, so it is not likely to represent realistic ROM, instead more conservative measurements were also taken and recorded in Table 2.

The ROM values for phalanx I-1 were supplemented with the physical manipulation and measurement of 3D printed models. Physical manipulations were able to reach much higher maximum extension and abduction angles when compared to the digital model (Table 2). The maximum abduction was recorded as 26 degrees, which closely matches the range reported for *Deinonychus* from a dissertation on *Deinonychus* forelimb functional morphology (Gishlick, 2002). ROM measurements for the other phalanx joints confirmed via physical measurements corroborated the digital results, so no further changes were necessary.

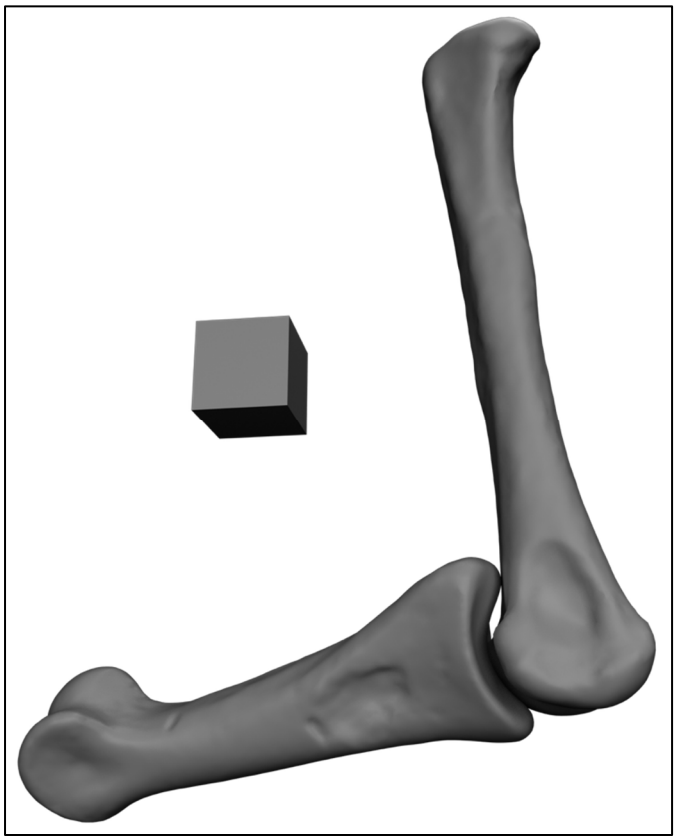

Figure 6: Example of a maximum-flexion manus joint. Note the phalanx appears to be disarticulated at this angle.

Realistic Forelimb Resting Pose

Once fully assembled the forelimb elements and joints in this study form the most complete reconstruction of a *Troodon* forelimb that has been made to date. However, once assembled the JCS 'zero-position' have the forelimb held in an unnatural position (Figure 5: e,f). This makes for easier joint measurement but doesn't reflect a realistic orientation that *Troodon* would use to rest its forelimb. Figure 7 is a more realistic representation of a *Troodon* resting orientation. This pose was based off skeletal findings from Senter and Robins, 2015, and was made by orienting each JCS within the ROM limits determined in this study (Table 2). The wrist

position and placement for the floating elements from digit III could not be based off joint systems, and instead were based off complete forelimb elements from related species, especially *Deinonychus* and *Bambiraptor* (Gishlick, 2002; Ostrom, 1969; Senter, 2006).

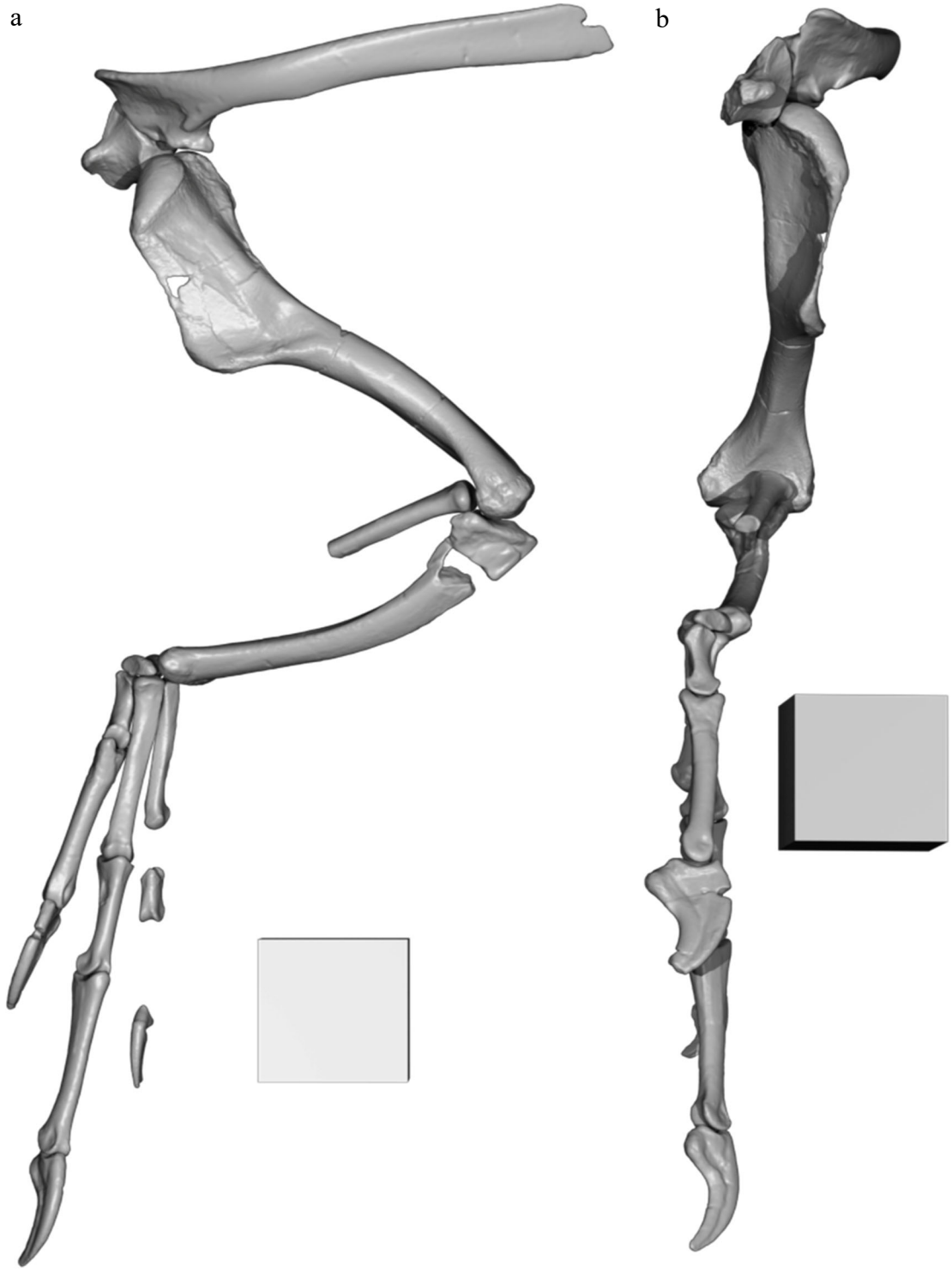

Figure 7: Realistic forelimb pose for *Troodon* in a) lateral and b) anterior view. Limb orientation based on work by Senter and Robins, 2015 and made with the ROM determined from this study.

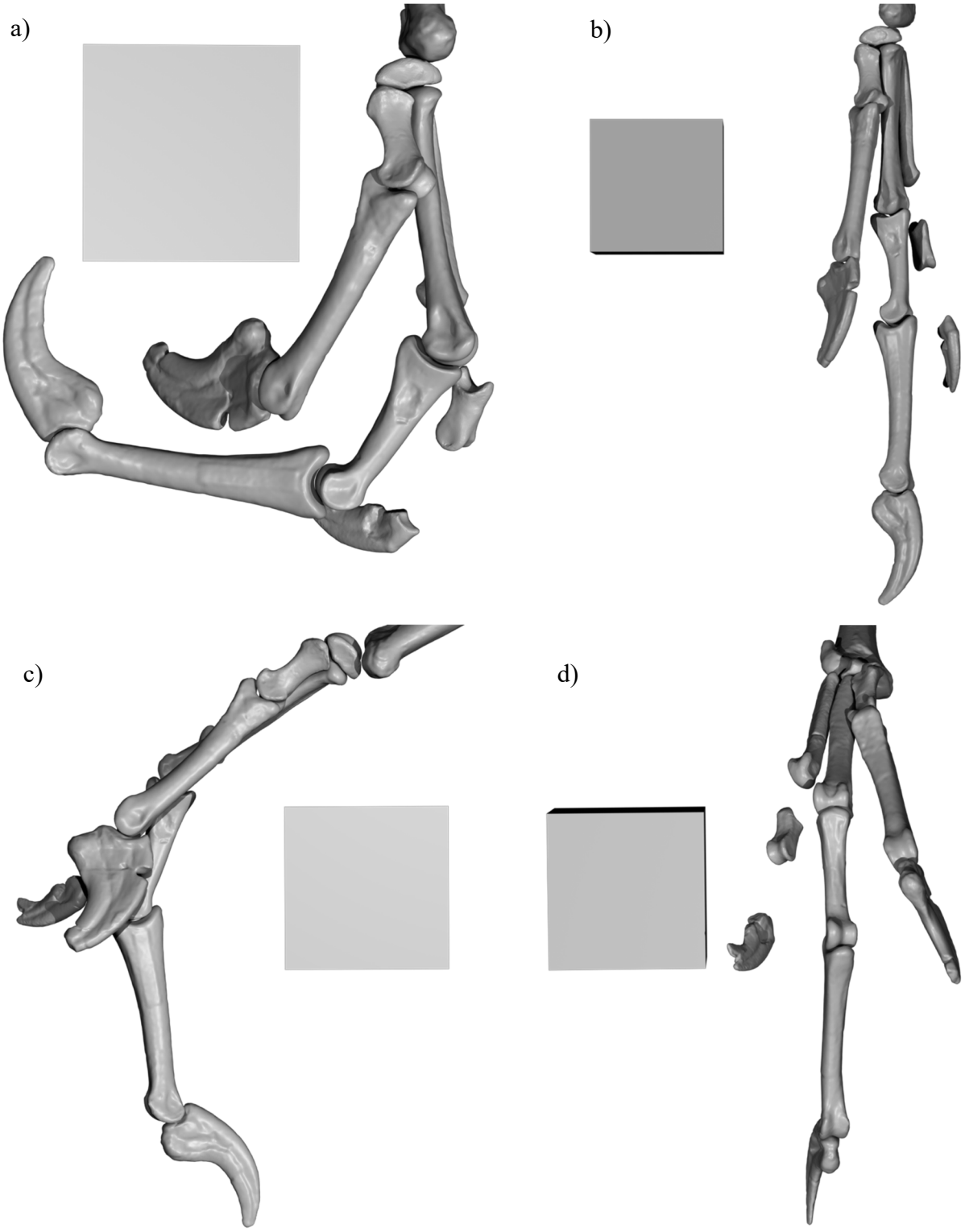

Figure 8: Closeup of *Troodon* manus in a) flexion, b) zero, and c) d) extension positions. Scale cube is 5 cm.

DISCUSSION

Whole Forelimb ROM and Hypothesis Testing

This reconstruction has allowed for the assembly of a nearly complete *Troodon* forelimb, and for the analysis of whole forelimb ROM hypotheses. The work of Dr. Phil Senter (Senter, 2006) has provided a framework for analyzing functional movement hypotheses. The functional hypotheses used in Dr Senter's study were used for the creation of the table for this study, with minor changes as noted in Table 3. The table includes potential actions, and a set of predictions that serve as mobility and ROM requirements for the action in question. Each prediction is checked against the measured ROM data and is either falsified or deemed plausible. Since each prediction serves as a prerequisite for the action in question, if any predictions are falsified the entire action is falsified as well. Importantly, since bone-on-bone ROM studies struggle with verifying true-to-life ROM and mobility the failure to falsify a hypothesis doesn't necessarily confirm that it could have been performed by the living animal in question. See Table 3 below for the functional hypotheses tested in this study.

Single and Double Handed Apprehension

Of particular interest to this study was the potential for single and double handed apprehension of objects, especially eggs. Eggs found from the Two Medicine Formation containing *Troodon* embryos have been described in detail (Varricchio, et al., 2002), with the dimensions of the eggs well known (Varricchio, et al., 2013). The dimensions of the *Troodon* eggs described in literature were compared to the reconstructed adult manus prepared for this study and were assessed for viability according to the hypotheses laid out in (Senter 2006).

Troodon eggs are oblong and taper at the base with one example, MOR 299, measured at 138 mm tall and a maximum width of 67 mm (Varricchio et al., 2013). The minimum measured distance across the manus when fully flexed was approximately 79 mm and involved the ungual phalanx from digit I nearly overlapping with digit II. The addition of digit III, as well as soft tissue and keratin may add additional support and cushion, however within the bounds of this study the one-handed grasping of its own eggs by *Troodon* cannot be confirmed. Two handed apprehension of eggs and other objects, however, remains plausible.

Table 3: Hypotheses and Prediction Table for *Troodon* Forelimb Movement

#	Hypotheses and Predictions, From Senter 2006	Falsified?
1	Both hands together can be used to grip and maintain hold upon an object, with palms and/or palmar surfaces of fingers as the primary organs of prehension.	
	Prediction 1: The joints of the forelimb permit the palms to face medially.	
	Prediction 2: The joints of the forelimb permit the palms to approach each other medially.	
	Prediction 3: The animal is capable of supporting itself bipedally.	
2	Both hands together can be used to grip and maintain hold upon an object, with claws as the primary organs of prehension.	
	Prediction 1–3: Same as those of Hypothesis 1.	
	Prediction 4: The unguals are recurved and sharp.	
	Prediction 5: The joints of the forelimb permit the unguals to be oriented with their tips toward the object.	
	Prediction 6: The unguals are capable of enough flexion to drive their tips into the object.	
3	One hand by itself can be used to grip an object by curling the fingers around the object.	**X**
	Prediction 1: The fingers are long enough to wrap at least halfway around the object.	X
	Prediction 2: The fingers are capable of enough flexion to press the object against the palm.	X
4	One hand by itself can be used to grip an object between the palmar surfaces of opposing fingers.	**X**
	Prediction 1: At least one finger is opposable to at least one other finger.	X for digits I and II
	Prediction 2: The object is small enough to grip between the opposable fingers.	
5	The hand can be used as a hook, to bring objects closer to the body.	
	Prediction 1: The fingers are capable of enough flexion to form an effective hook.	
	Prediction 2: The length and joints of the forelimb permit the hand to be brought near the body while the fingers are flexed (that is, they do not constrain the forelimb to an extended position).	
6	The forelimb can be used to bring an object to the mouth.	
	Prediction 1: The joints of the forelimb permit the forelimb to reach the mouth.	
	Prediction 2: At least one of the following supported: Hypotheses 1-5.	
7	The forelimbs can be used to perform a display that involves extending the forelimbs and swinging them dorsoventrally, above the spine.*	
	Prediction 1: The joints of the forelimb allow the limb to be extended.	
	Prediction 2: The shoulder joint permits the humerus to swing in a large, transverse arc.	
	Prediction 3: The forelimb can be lifted above the spine dorsally.*	

Table 3 Continued: Hypotheses and Prediction Table for *Troodon* Forelimb Movement

8 The forelimbs can be used to perform a display that involves extending the forelimbs and swinging them craniocaudally.	
Prediction 1: The joints of the forelimb allow the limb to be extended.	
Prediction 2: The shoulder joint permits the humerus to swing in a large, parasagittal arc.	
9 The forelimbs can be used to clutch objects to the chest.	
Prediction 1: At least one of the following is supported: Hypotheses 3–7.	
Prediction 2: The humerus can be retracted so that the elbow is level with the ventral surface of the torso.	
Prediction 3: The joints of the forelimb allow the elbow to flex when the humerus is retracted.	
Prediction 4: If the antebrachia are long, the elbow can flex to a strongly acute angle.	
Prediction 5: The animal is capable of supporting itself bipedally.	
10 The hand can be used to probe small crevices, e.g. to extract food items (as in the extant aye-aye).	**X**
Prediction 1: At least one finger is elongate and narrow (Von Koenigswald et al., 1992).	
Prediction 2: At least one of the following is true: (1) The other fingers are capable of enough flexion or extension to move out of the way so that the probing finger can enter deep into the crevice, (2) the probing finger is capable of enough flexion or extension to move out of the way of the other fingers, (3) or the probing finger is much longer than the other fingers.	
Prediction 3: The probing finger is unobstructed by integumentary appendages.	X (only if digit II bore feathers)
* Hypothesis or prediction modified from Senter, 2006	

Comparative Range of Motion

Comparisons with Traditional Studies

Table 4 shows a list of forelimb flexion and extension angles for the shoulder, antebrachium and manus for several species of theropods, including *Troodon*. All the studies included in Table 4 used bone-on-bone approaches to measure joint angles, with some using physical bones (Senter & Parrish, 2005; Senter 2006; Senter & Sullivan 2021) and others using

digital scans of bones (White et al., 2015; Yu et al., 2022). While there is a mix of physical and digital studies, none of the included studies used the JCS creation process to create their joints, instead they all used manual manipulations. This is a stark difference from this study, that used the JCS to orient joints and measure ROM. This can make joint comparisons complicated, since the joint axes between manual and JCS studies can differ. For JCS studies the axes are largely dependent on the 'zero-position' of the model, which in turn is decided by the X axis orientation. To allow for the most overlap in axes placement with the manual ROM studies this study oriented the X axes for each joint down the long axis of each bone pointing distally, which orients each joint in a straight line (Figure 5: e,f). This approach matched the traditional manual ROM axes for all the manual joints, but there was some deviation with the elbow and shoulder.

The elbow joint ROM in traditional ROM studies is measured by taking the angle created between the humerus and ulna/radius when in maximum flexion and subtracting it from the angle created when the antebrachium is in maximum extension. This 'subtractive' approach obviates the need for a 'zero-position' when measuring the antebrachium but makes it difficult to compare with the ACS results. This means that the flexion and extension ROM results cannot be compared between this study and the other traditional studies included in Table 4. However, the total ROM for the antebrachium (bolded values in Table 4) between this and other studies can be compared, as both values represent the maximum arc that the ulna and radius take about the humerus.

The shoulder results from this study are the most complicated to draw comparisons. The humeral head shows evidence for movements more complicated than a simple hinge joint. Since this simplification was used for every joint in this study, the shoulders movements are likely

oversimplified. As such the ROM results should not be used as a direct 1:1 comparison with other studies, but more to get a general idea for preferred planes and orientations of movement.

Flexion and Extension Comparisons

Yu et al., 2022 acknowledged the trend in generally increasing flexion and decreasing extension when moving closer to paravian and true avialan dinosaurs. *Troodon* supports this trend generally, showing flexion within a reasonably close range of ~20 degrees, especially for closely related species (except for the Mongolian troodontid described in Yu et al., 2022). However, *Troodon* shows a greatly increased range of extension, especially within the manus, when compared to other closely related and well represented species within paravian dinosaurs. The articulated surfaces for the manus bones used in this study are in excellent shape, easily reflecting the potential path of movement for each element, so taphonomic, or other alterations of the bone surface is likely not resulting in this extension increase. The digital marionet produced to measure joint angles digitally could result in an overestimation of extension. Manus joint angles were verified by hand with 3D printed copies and measured via protractor to roughly confirm digitally determined angles, and matched most joints analyzed, unless noted in Table 2. If this increase in extension ROM is valid, it reflects a reversal by *Troodon* from the previously noted trend and may indicate a deviation in hunting behavior or general forelimb utility relative to other members of Paraves.

Interestingly, the flexion and extension ROM for the *Troodon* manus is unexpectedly higher than the Mongolian troodontid manus described in Yu et al., 2022, specifically for digit II. Reviewing the condition of bones described and analyzed, the Mongolian specimens are crushed and, in some cases, altered well beyond the specimens for *Troodon*. This could be an explanation

for the high deviation in ROM. Given the geographic separation of Asian and North American troodontid species, it is plausible that the two groups of troodontids had different manus morphologies. However, this hypothesis will be difficult to test without more Mongolian and North American forelimb specimens.

Table 4: Comparative Forelimb ROM Table

Comparative Forelimb ROM Chart, Modifed from Yu et al., 2022, White et al., 2015								
Dinosaur Taxon Source		**Shoulder**	**Ante-brachium***	**I-1**	**I-2**	**II-1**	**II-2**	**II-3**
Troodon formosus (MOR 563, 553)	Extension	81.42	25.05	25.00	28.79	35.50	29.4	36.24
	Flexion	85.97	116.54	42.48	65.69	47.69	60.10	65.56
	Total ROM	**167.39**	**141.59**	**67.48**	**94.48**	**83.19**	**89.48**	**101.80**
SDUST-V1042 (Unnamed troodontid) Yu et al., 2022	Extension	-	-	-	-	-	4	0
	Flexion	-	-	-	~71	-	32	9
	Total ROM	**-**	**-**	**-**	**-**	**-**	**36**	**9**
Deinonychus antirrhopus Senter & Parrish, 2005; Senter, 2006	Extension	-	150	43	4	10	0	11
	Flexion	-	51	49	70	51	75	85
	Total ROM	**-**	**99**	**92**	**74**	**61**	**75**	**96**
Bambiraptor feinbergi Senter & Parrish, 2005; Senter, 2006	Extension	33	127, 136	15	0	28	7	6
	Flexion	88	59, 55	51	76	50	70	92
	Total ROM	**121**	**68, 81**	**66**	**76**	**78**	**77**	**98**
Chirostenotes pergracilis Senter & Parrish, 2005	Extension	-	-	5	7	24	25, 16	4
	Flexion	-	-	51	62	41	58, 60	52
	Total ROM	**-**	**-**	**56**	**69**	**65**	**83, 76**	**56**
Gallimimus sp. Senter & Parrish, 2005; Kobayashi & Barsbold, 2005	Extension	-	-	20	0	25	0	0
	Flexion	-	-	33	96	27	33	90
	Total ROM	**-**	**-**	**53**	**96**	**52**	**33**	**90**
Ornitholestes hermanni Senter & Parrish, 2005; Senter, 2006(b)	Extension	-	148	29	0	-	-	17
	Flexion	-	53	52	85	-	-	100
	Total ROM	**-**	**95**	**81**	**85**	**-**	**-**	**117**
Harpymimus okladnikovi Senter & Parrish, 2005; Kobayashi & Barsbold, 2005	Extension	-	-	28	0	19	14	0
	Flexion	-	-	70	97	25	46	90
	Total ROM	**-**	**-**	**98**	**97**	**44**	**60**	**90**
Guanlong wucaii Yu et al., 2015	Extension	-	-	49	10	46	22	28
	Flexion	-	-	31	71	31	72	33
	Total ROM	**-**	**-**	**80**	**81**	**77**	**94**	**61**
Tyrannosaurus rex Senter & Parrish, 2005; Carpenter & Smith, 2001	Extension	-	-	35	34	-	-	-
	Flexion	-	-	18	22	-	-	-
	Total ROM	**-**	**45**	**53**	**56**	**-**	**-**	**-**
Australovenator wintonensis White et al., 2015	Extension	-	144	40	42	38	37	37
	Flexion	-	66	10	80	36	31	73
	Total ROM	**-**	**78**	**50**	**122**	**74**	**68**	**110**

Table 4 Continued: Comparative Forelimb ROM Table

Acrocanthosaurus atokensis Senter & Robins, 2005	Extension	24	159	90	0	77	97	0
	Flexion	109	104	35	3	36	70	35
	Total ROM	**133**	**55**	**125**	**3**	**113**	**167**	**35**
Allosaurus fragilis Senter & Parrish, 2005; Carpenter, 2001	Extension	-	-	55	-	20	10	0
	Flexion	-	-	19	-	18	63	58
	Total ROM	**-**	**62**	**74**	**-**	**38**	**73**	**58**
Dilophosaurus wetherilli Senter & Sullivan, 2019	Extension	-	150	19	28	105	-	18
	Flexion	-	102	16	65	21	-	27
	Total ROM	**85**	**48**	**35**	**93**	**126**	**-**	**45**
Coelophysis bauri Senter & Parrish, 2005	Extension	-	-	18	26	17	13	10
	Flexion	-	-	54	40	48	60	50
	Total ROM	**-**	**-**	**72**	**66**	**65**	**73**	**60**

* *Troodon* antebrachium ROM measurment is additive, other studies referenced are subtractive
'-' no value reported, '~' estimated value

Forelimb Morphology

Musculature and Mechanical Properties

The whole forelimb reconstruction for *Troodon* (Figure 7) is robust and stout, especially when compared within troodontidae, specifically the humerus. Unlike most other paravian species, *Troodon's* humerus is stocky and thick, with the deltopectoral crest (DPC) taking up nearly half the length of the shaft. This contrasts sharply with related paravian species like *Deinonychus, Archaopteryx, Gobivenator* and *Mei,* which all have a DPC roughly a quarter the length of the humeral shaft (Ostrom, 1969; Voetan et al., 2018; Tsuihiji et al., 2014; Gao et al., 2012). Looking outside of Paraves the *Troodon* humerus is more similar to those of larger theropods, like *Allosaurus* (Madsen, 1975; Figure 9).

Numerous studies have detailed the muscle connections in the DPC including the connection of the pectoralis, coracobrachialis and supracoracoideus muscle systems (Burch, 2014; Jasinoski et al., 2006). Generally, these muscles act on the humerus via the DPC. The

position of the DPC has a tremendous effect on the mechanical leverage that the muscles can produce on the humerus. The humerus operates akin to a type 3 lever, with the fulcrum (humeral head) acted on by muscle attachments in the DPC (force) that results in movement at the humeral condyle (load; The Oxford Dictionary of Sports Science and Medicine). Long humeri with short DPC's, like *Deinonychus* and *Bambiraptor,* work like a lever with the force located close to the fulcrum. This mechanically produces a long movement arm, which excels at moving quickly, but sacrifices maximum torque (Gardner et al., in review). Shorter humeri with longer DPC's, like *Troodon*, perform in an opposite fashion, with the force applied further away from the fulcrum, producing shorter moment arms, and moving at lower speeds, but with higher maximum torque. High torque systems produce higher force and may indicate a deviation in forelimb utility and hunting strategy of *Troodon* relative to closely related species. If connected, this could indicate that *Troodon* was using its forelimbs to grasp and hold onto potentially struggling prey items, utilizing the higher strength allowed by its forearms.

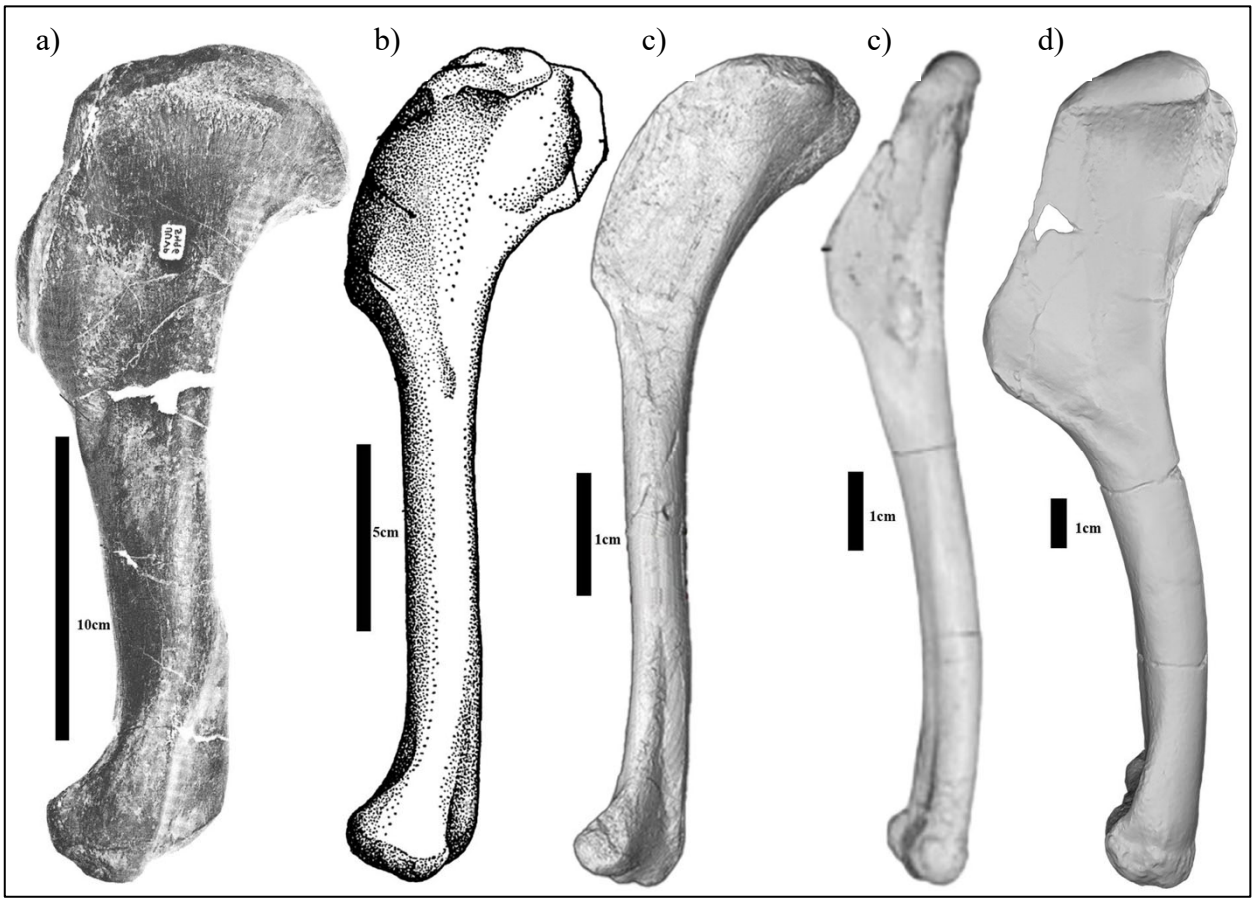

Figure 9: Humerus comparison comparing a) *Allosaurus* (Madsen, 1975), b) *Deinonychus*, (Ostrom, 1969), c) *Archaeopteryx* (Voetan et al., 2018), d) *Gobivenator* (Tsuihiji et al., 2014), e) *Troodon* (this study).

Digit Opposability and One Hand Grasping

Based on the mobility of digits I and II, the hypothesis that *Troodon* could pick up objects the same size and shape as its own eggs with one hand was falsified, as was the potential for digit opposability. Interestingly, the flexion movement of digit I brings it towards the midline of the manus, a pattern that was described by Dr. Phil Senter when analyzing the manual ROM for *Bambiraptor* (Senter, 2006). In his study, Dr. Senter was able to show that digit I approached digit III at maximum flexion when digit II was out of the way. If *Troodon* follows the same

pattern, it may indicate the potential for more flexibility in one-handed grasping than was confirmed by this study. It bears repeating that just because an animal could follow a certain ROM doesn't indicate whether it would take that action in life. However, it is also worth noting that while this study falsified the hypotheses regarding one handed grasping, the discovery and description of digit III in *Troodon* may update this in the future.

Benefits and Drawbacks of Physical and Digital ROM Approaches

Physical ROM

Through the process of printing physical copies of the digital bones, numerous benefits were observed. It was less obvious in the initial digital reconstruction and scaling, but the scapula and coracoid were initially incorrectly scaled. The scapula was first scaled based on the greatest length of the element but was incomplete. The awkward scaling was much easier to identify when physical copies of the scapula and coracoid could be compared to the physical copy of the humerus. Once identified it was an easy fix to rescale the scapula based on its more complete distal width. Additionally, the freedom of manipulating the bones by hand helped to quickly check joint manipulations. The first joint on digit I has a different morphology when compared to the other joints in the manus. This made understanding its preferred orientations and pathways digitally challenging, and in some cases resulted in premature bone-on-bone contact and overlap. Being able to hold metacarpal I and phalanx I-1 by hand to test the ROM provided a much-needed check on the digital system and was able to identify more range than initially assumed.

However, when compared to digital methods physical ROM can come up short. For example, studies are largely limited to studying complete specimens, with little that can be done

with missing and incomplete specimens. Physical methods are also limited in scope, restricted only to measuring skeletal movement, while digital models can add soft tissue, and even muscle (Heers et al., 2018; Burch, 2014).

Digital ROM

Most of the fossil specimens included in this reconstruction were from multiple individuals at different stages of growth and different sides of the body. For traditional ROM analysis that rely upon whole or associated elements these specimens could not have been used. Additionally, certain elements were broken or incomplete but were digitally amended, in some cases combining parts from multiple elements into one (Table 1). While combining multiple elements from different individuals does carry uncertainties, these techniques allow for the analysis of specimens that would have been previously overlooked.

The digital methods are also not without their drawbacks as well. The first and largest obstacle to taking up digital ROM methods is the equipment needed. The latest scanning technology and CT scans can create large files that require a specialized, and often dedicated, machine to run. Adding on top of that the barrier of entry presented by complicated digital modeling software, and the learning curve and time commitment becomes higher than a standard physical ROM assessment. Additionally, considering the relative novelty of the digital approaches in development there isn't as much standardization for the process as there has been with traditional ROM approaches. However, as work continues in this field standard practice will solidify and things will steadily become easier to adopt (Bishop et al., 2021; Gatesy et al., 2022; Manafzadeh et al., 2022).

Areas of Uncertainty

Scaling

As described previously, the techniques required to scale each bone into a representative forelimb varied slightly from element to element. Depending on element completion and association with other elements scaling became more complicated and introduced with it more uncertainty. As such, not every element used in this reconstruction can be held at the same level of certainty. The scaling process for each element is described at length in the Materials section, however for ease of reference Table 1 also includes the relative certainty next to each scaled element.

Ontogeny. As *Troodon* grew, the morphology of its forelimb bones largely remained the same. However, as was shown by the humerus, adult bones do grow more robust and stocky overtime. Documenting the exact ontogenetic changes in *Troodon* hasn't yet been published, so understanding the tradeoffs with scaling smaller elements is unclear. Bones like the semilunate carpal, scapula and radius were up-scaled more than other elements, but all appear to fit the current reconstruction without issue.

Shoulder

The shoulder joint posed a unique challenge, as the JCS creation process assumed that each joint operated like a hinge, but the articular surface for the humeral head does not follow this simplified geometry. As such, the overall ROM may be overestimated for some angles, and underestimated in others. It's also clear after observing the spacing in the glenoid relative to the humeral head that soft tissues also play an important role in the ROM of the shoulder, so a bone-

on-bone approach likely has a lot of uncertainty. Keeping this in mind, the abduction and adduction measurements are likely underestimated for this joint. It is also worth noting that there was bone-on-bone contact recorded prior to the maximum flexion angle, but it was ultimately disregarded for this study due to the likelihood that soft tissue would have prevented contact.

Wrist

The wrist was the only joint outside of digit III that could not be analyzed for this study. Without the distal radius or radiale bone, the exact placement and orientation of the semilunate carpal, and by extension the manus, could not be made by bone orientation alone. Instead, other related species were referenced, especially *Deinonychus*, in orienting the metacarpus and manus into as realistic a position as possible (Gishlik, 2002; Ostrom, 1969). Finally, without the wrist, the full medial and lateral ROM of the manus could not be tested in this study, and so was left out of hypothesis testing and ROM analysis.

Joint Spacing

Initially, joint spacing was going to be added to each joint by following Hutchinson et al,. 2005. However, after testing the spacing on the forelimb joints, they appeared to be too extreme. Applying hindlimb soft tissue data to forelimbs, especially in bipedal animals, would appear to be unrealistic. Future work into realistic soft tissue spacing for forelimb joints in bipedal dinosaurs will be necessary to help address this gap, including potential study of bipedal animals outside of Archosauria. Additional obstacles to standardizing joint spacing includes the ease of assembling and testing a bone-on-bone study using physical specimens. This ease of use is why bone-on-bone methods have been the traditional standard for forelimb ROM studies. This

standard is another obstacle to the adoption of joint spacing, as the traditional bone-on-bone studies aren't comparable to those with spacing, limiting the potential for comparative study.

CONCLUSION

This study is the first forelimb reconstruction and ROM assessment performed for the theropod dinosaur *Troodon formosus*. Leveraging digital scanning and 3D printing technology, the disassociated skeletal forelimb elements from multiple individuals of *Troodon* were assembled into a single forelimb representative of a nearly complete adult arm and hand. Due to missing elements, digit III and the wrist were left out of the ROM study, but the rest of the forelimb was analyzed for the first time.

Troodon, like similarly related member of Paraves, shows increased flexion in its forelimb joints relative to extension. However, *Troodon* shows much higher extension when compared to closely related groups. Additionally, *Troodon* has a much stockier built forelimb when compared within Paraves and even within other troodontids, potentially indicating a deviation in hunting strategy or forelimb usage. Based on ROM results, one handed grasping of objects, especially eggs, by *Troodon* has been falsified, but future material could update this result.

More work into the soft tissue spacing in the forelimbs of bipedal theropod dinosaurs requires more attention in future studies. The extent that soft tissue affects the ROM of the shoulder joint also requires future attention. This study also combined the use of digital and physical specimens to aid in the bone-on-bone ROM measurement of *Troodon's* forelimb. Further work into the potential overlap of digital and physical methods will likely prove to be synergistic in this area of ROM study.

This study has helped reveal specialization in *Troodon's* forelimbs, and potential implications related to feeding and reproductive behavior. Further material collection and study

will hopefully round out what we know about *Troodon* and help further reveal the peculiarities of this enigmatic theropod.

REFERENCES CITED

Baier, D. B., & Gatesy, S. M. (2013). Three-dimensional skeletal kinematics of the shoulder girdle and forelimb in walking *Alligator*. *Journal of Anatomy*, *223*(5), 462–473. https://doi.org/10.1111/joa.12102

Bishop, P. J., Cuff, A. R., & Hutchinson, J. R. (2021). How to build a dinosaur: Musculoskeletal modeling and simulation of locomotor biomechanics in extinct animals. *Paleobiology*, *47*(1), 1–38. https://doi.org/10.1017/pab.2020.46

Burch, S. H. (2014). Complete forelimb myology of the basal theropod dinosaur *Tawa hallae* based on a novel robust muscle reconstruction method. *Journal of Anatomy*, *225*(3), 271–297. https://doi.org/10.1111/joa.12216

Carpenter, K. (2002). Forelimb biomechanics of nonavian theropod dinosaurs in predation. *Senckenbergiana Lethaea*, *82*(1), 59–75. https://doi.org/10.1007/BF03043773

Charles M. Sternberg. (1932). Two New Theropod Dinosaurs from The Belly River Formation of Alberta. *The Canadian Field-Naturalist*, *46*(5), 99–105.

Charles M. Sternberg. (1945). Pachycephalosauridae Proposed for Dome-Headed Dinosaurs, *Stegoceras lambei*, n. Sp., Described. *Journal of Paleontology*, *19*(5), 534–538.

Currie, P. J. (1987). Bird-like characteristics of the jaws and teeth of troodontid theropods (Dinosauria, Saurischia). *Journal of Vertebrate Paleontology*, *7*(1), 72–81. https://doi.org/10.1080/02724634.1987.10011638

Fearon, Jamie Lynn. (2013). *SCRATCH-DIGGING IN THE CRETACEOUS BASAL ORNITHOPOD DINOSAUR ORYCTODROMEUS CUBICULARIS: EVIDENCE FROM MORPHOMETRIC ANALYSES AND RECONSTRUCTION OF THE FORELIMB MUSCULATURE*. Montana State University.

Fowler, D. W. (2017). Revised geochronology, correlation, and dinosaur stratigraphic ranges of the Santonian-Maastrichtian (Late Cretaceous) formations of the Western Interior of North America. *PLOS ONE*, *12*(11), e0188426. https://doi.org/10.1371/journal.pone.0188426

Freimuth, W. J., Varricchio, D. J., Brannick, A. L., Weaver, L. N., & Wilson Mantilla, G. P. (2021). Mammal-bearing gastric pellets potentially attributable to *Troodon formosus* at the Cretaceous Egg Mountain locality, Two Medicine Formation, Montana, USA. *Palaeontology*, *64*(5), 699–725. https://doi.org/10.1111/pala.12546

Galton, Peter M. (1971). Manus movements of the coelurosaurian dinosaur *Syntarsus* and opposability of the theropod hallux. *Arnoldia*, *5*(15), 1–8.

Gao, C., Morschhauser, E. M., Varricchio, D. J., Liu, J., & Zhao, B. (2012). A Second Soundly Sleeping Dragon: New Anatomical Details of the Chinese Troodontid *Mei long* with Implications for Phylogeny and Taphonomy. *PLoS ONE*, *7*(9), e45203. https://doi.org/10.1371/journal.pone.0045203

Gatesy, S. M., Baier, D. B., Jenkins, F. A., & Dial, K. P. (2010). Scientific rotoscoping: A morphology-based method of 3-D motion analysis and visualization. *Journal of Experimental Zoology Part A: Ecological Genetics and Physiology*, *9999A*, n/a-n/a. https://doi.org/10.1002/jez.588

Gatesy, S. M., Manafzadeh, A. R., Bishop, P. J., Turner, M. L., Kambic, R. E., Cuff, A. R., & Hutchinson, J. R. (2022). A proposed standard for quantifying 3-D hindlimb joint poses in living and extinct archosaurs. *Journal of Anatomy*, *241*(1), 101–118. https://doi.org/10.1111/joa.13635

Gill, J. & Coban, W. (1973). Stratigraphy and geologic history of the Montana Group and equivalent rocks, Montana, Wyoming and North and South Dakota. *USGS Prof. Pap.*, *776*.

Gilmore, Charles W. (1924). On *Troodon validus*, an orthopodous dinosaur from the Belly River Cretaceous of Alberta, Canada. *Department of Geology, University of Alberta Bulletin*, *1*, 1–43.

Gishlick, Alan D. (2002). The Functional Morphology of the Forelimb of *Deinonychus antirrhopus* and its Importance for the Origin of Avian Flight [Dissertation]. Yale University.

Grood, E. S., & Suntay, W. J. (1983). A Joint Coordinate System for the Clinical Description of Three-Dimensional Motions: Application to the Knee. *Journal of Biomechanical Engineering*, *105*(2), 136–144. https://doi.org/10.1115/1.3138397

Heers, A. M., Rankin, J. W., & Hutchinson, J. R. (2018). Building a Bird: Musculoskeletal Modeling and Simulation of Wing-Assisted Incline Running During Avian Ontogeny. *Frontiers in Bioengineering and Biotechnology*, *6*, 140. https://doi.org/10.3389/fbioe.2018.00140

Herbst, E. C., Manafzadeh, A. R., & Hutchinson, J. R. (2022). Multi-Joint Analysis of Pose Viability Supports the Possibility of Salamander-Like Hindlimb Configurations in the Permian Tetrapod *Eryops megacephalus*. *Integrative and Comparative Biology*, *62*(2), 139–151. https://doi.org/10.1093/icb/icac083

Holliday, C. M., Ridgely, R. C., Sedlmayr, J. C., & Witmer, L. M. (2010). Cartilaginous Epiphyses in Extant Archosaurs and Their Implications for Reconstructing Limb Function in Dinosaurs. *PLoS ONE*, *5*(9), e13120. https://doi.org/10.1371/journal.pone.0013120

Hutchinson, J. R., Anderson, F. C., Blemker, S. S., & Delp, S. L. (2005). Analysis of hindlimb muscle moment arms in *Tyrannosaurus rex* using a three-dimensional musculoskeletal computer model: Implications for stance, gait, and speed. *Paleobiology*, *31*(4), 676–701.

Jasinoski, S. C., Russell, A. P., & Currie, P. J. (2006). An integrative phylogenetic and extrapolatory approach to the reconstruction of dromaeosaur (Theropoda: Eumaniraptora) shoulder musculature. Zoological Journal of the Linnean Society, 146(3), 301–344. https://doi.org/10.1111/j.1096-3642.2006.00200.x

Kambic, R. E., Roberts, T. J., & Gatesy, S. M. (2014). Long-axis rotation: A missing degree of freedom in avian bipedal locomotion. *Journal of Experimental Biology*, jeb.101428. https://doi.org/10.1242/jeb.101428

Leidy, J. (1860). Extinct Vertebrata from the Judith River and Great Lignite Formations of Nebraska. *Transactions of the American Philosophical Society*, *11*, 139. https://doi.org/10.2307/3231936

Lipkin, C., & Carpenter, K. (2008). LOOKING AGAIN AT THE FORELIMB OF *TYRANNOSAURUS REX*. In *Tyrannosaurus rex, the tyrant king* (pp. 166–190). lndiana University Press.

James H. Madsen. (1993). *Allosaurus Fragilis*: A Revised Osteology. Utah Geologica Survey.

Mallison, H. (2010). CAD assessment of the posture and range of motion of *Kentrosaurus aethiopicus* Hennig 1915. *Swiss Journal of Geosciences*, *103*(2), 211–233. https://doi.org/10.1007/s00015-010-0024-2

Manafzadeh, A. R., & Gatesy, S. M. (2021). Paleobiological reconstructions of articular function require all six degrees of freedom. *Journal of Anatomy*, *239*(6), 1516–1524. https://doi.org/10.1111/joa.13513

Manafzadeh, A. R., & Gatesy, S. M. (2022). Advances and Challenges in Paleobiological Reconstructions of Joint Mobility. *Integrative and Comparative Biology*, icac008. https://doi.org/10.1093/icb/icac008

Manafzadeh, A. R., & Padian, K. (2018). ROM mapping of ligamentous constraints on avian hip mobility: Implications for extinct ornithodirans. *Proceedings of the Royal Society B: Biological Sciences*, *285*(1879), 20180727. https://doi.org/10.1098/rspb.2018.0727

McGookey, D. (1972). Cretaceous system. In *Geologic Atlas of the Rocky Mountain Region.* (pp. 190–228). Rocky Mountain Association of Geology, Denver.

Moore, B. R. S., Roloson, M. J., Currie, P. J., Ryan, M. J., Patterson, R. T., & Mallon, J. C. (2022). The appendicular myology of *Stegoceras validum* (Ornithischia: Pachycephalosauridae) and implications for the head-butting hypothesis. *PLOS ONE*, *17*(9), e0268144. https://doi.org/10.1371/journal.pone.0268144

Novas, F. E., & Puertat, P. F. (1997). New evidence concerning avian origins from the Late Cretaceous of Patagonia. *Nature*, *387*(6631), 390–392. https://doi.org/10.1038/387390a0

Franz Nopcsa. (1901). Synopsis un Abstammung der Dinosaurier. *Földtani Közlöny*, *31*, 247–288.

Ostrom, J. H. (1969). Osteology of *Deinonychus antirrhopus*, an Unusual Theropod from the Lower Cretaceous of Montana. *The Peabody Museum Bulletin*, *30*, 172.

Ramezani, J., Beveridge, T. L., Rogers, R. R., Eberth, D. A., & Roberts, E. M. (2022). Calibrating the zenith of dinosaur diversity in the Campanian of the Western Interior Basin by CA-ID-TIMS U–Pb geochronology. *Scientific Reports*, *12*(1), 16026. https://doi.org/10.1038/s41598-022-19896-w

Rogers, R.R., Swisher, C.C., & Horner, J.R. (1993). 4°Ar/39Ar age and correlation of the nonmarine Two Medicine Formation (Upper Cretaceous), northwestern Montana, U.S.A. *Canadian Journal of Earth Sciences*, *30*, 1066–1075.

Russell, Dale A. (1969). A new specimen of *Stenonychosaurus* from the Oldman Formation (Cretaceous) of Alberta. Canadian Journal of Earth Sciences, 6(4), 595–612.

Senter, P. (2005). Function in the stunted forelimbs of *Mononykus olecranus* (Theropoda), a dinosaurian anteater. *Paleobiology*, *31*(3), 373–381. https://doi.org/10.1666/0094-8373(2005)031[0373:FITSFO]2.0.CO;2

Senter, P. (2006a). FORELIMB FUNCTION IN *ORNITHOLESTES HERMANNI* OSBORN (DINOSAURIA, THEROPODA): FORELIMB FUNCTION IN A CRETACEOUS THEROPOD. *Palaeontology*, *49*(5), 1029–1034. https://doi.org/10.1111/j.1475-4983.2006.00585.x

Senter, P. (2006b). Comparison of forelimb function between *Deinonychus* and *Bambiraptor* (Theropoda: Dromaeosauridae). *Journal of Vertebrate Paleontology*, *26*(4), 897–906. https://doi.org/10.1671/0272-4634(2006)26[897:COFFBD]2.0.CO;2

Senter, P., & Robins, J. H. (2005). Range of motion in the forelimb of the theropod dinosaur *Acrocanthosaurus atokensis* , and implications for predatory behaviour. *Journal of Zoology*, *266*(3), 307–318. https://doi.org/10.1017/S0952836905006989

Senter, P., & Robins, J. H. (2015). Resting Orientations of Dinosaur Scapulae and Forelimbs: A Numerical Analysis, with Implications for Reconstructions and Museum Mounts. *PLOS ONE*, *10*(12), e0144036. https://doi.org/10.1371/journal.pone.0144036

Senter, P., & Sullivan, C. (2019). Forelimbs of the theropod dinosaur *Dilophosaurus wetherilli*: Range of motion, influence of paleopathology and soft tissues, and description of a distal carpal bone. *Palaeontologia Electronica*. https://doi.org/10.26879/900

Sereno, P. C. (1994). The Pectoral Girdle and Forelimb of the Basal Theropod *Herrerasaurus Ischigualastensis*. *Journal of Vertebrate Paleontology*, *13*(4), 425–450.

Sereno, P. C. (1999). The Evolution of Dinosaurs. Science, 284(5423), 2137–2147. https://doi.org/10.1126/science.284.5423.2137

Sullivan, C., Hone, D. W. E., Xu, X., & Zhang, F. (2010). The asymmetry of the carpal joint and the evolution of wing folding in maniraptoran theropod dinosaurs. *Proceedings of the Royal Society B: Biological Sciences*, *277*(1690), 2027–2033. https://doi.org/10.1098/rspb.2009.2281

Tsuihiji, T., Barsbold, R., Watabe, M., Tsogtbaatar, K., Chinzorig, T., Fujiyama, Y., & Suzuki, S. (2014). An exquisitely preserved troodontid theropod with new information on the palatal structure from the Upper Cretaceous of Mongolia. Naturwissenschaften, 101(2), 131–142. https://doi.org/10.1007/s00114-014-1143-9

Varricchio, D. J. (1993). Bone microstructure of the Upper Cretaceous theropod dinosaur *Troodon formosus*. *Journal of Vertebrate Paleontology*, *13*(1), 99–104. https://doi.org/10.1080/02724634.1993.10011490

Varricchio, D. J. (1995). Taphonomy of Jack's Birthday Site, a diverse dinosaur bonebed from the Upper Cretaceous Two Medicine Formation of Montana. *Palaeogeography, Palaeoclimatology, Palaeoecology*, *114*(2–4), 297–323. https://doi.org/10.1016/0031-0182(94)00084-L

Varricchio, D. J., Jackson, F., Borkowski, J. J., & Horner, J. R. (1997). Nest and egg clutches of the dinosaur *Troodon formosus* and the evolution of avian reproductive traits. *Nature*, *385*(6613), 247–250. https://doi.org/10.1038/385247a0

Varricchio, D. J., Jackson, F., & Trueman, C. N. (1999). A nesting trace with eggs for the Cretaceous theropod dinosaur *Troodon formosus*. *Journal of Vertebrate Paleontology*, *19*(1), 91–100. https://doi.org/10.1080/02724634.1999.10011125

Varricchio, D. J., Horner, J. R., & Jackson, F. D. (2002). Embryos and eggs for the Cretaceous theropod dinosaur *Troodon formosus*. *Journal of Vertebrate Paleontology*, *22*(3), 564–576. https://doi.org/10.1671/0272-4634(2002)022[0564:EAEFTC]2.0.CO;2

Varricchio, D. J., Jackson, F. D., Jackson, R. A., & Zelenitsky, D. K. (2013). Porosity and water vapor conductance of two *Troodon formosus* eggs: An assessment of incubation strategy in a maniraptoran dinosaur. *Paleobiology*, *39*(2), 278–296. https://doi.org/10.1666/11042

Varricchio, D. J., Jin, X., & Jackson, F. D. (2015). Lay, brood, repeat: Nest reuse and site fidelity in ecologic time for two Cretaceous troodontid dinosaurs. *Journal of Vertebrate Paleontology*, *35*(3), e932797. https://doi.org/10.1080/02724634.2014.932797

Varricchio, D.J., Hogan, J.D., & Freimuth, W.J. (2021). Revisiting Russell's troodontid: Autecology, physiology, and speculative tool use. Canadian Journal of Earth Sciences, 58(9), 796–811.

Voeten, D. F. A. E., Cubo, J., de Margerie, E., Röper, M., Beyrand, V., Bureš, S., Tafforeau, P., & Sanchez, S. (2018). Wing bone geometry reveals active flight in *Archaeopteryx*. Nature Communications, 9(1), 923. https://doi.org/10.1038/s41467-018-03296-8

White, M. A., Bell, P. R., Cook, A. G., Barnes, D. G., Tischler, T. R., Bassam, B. J., & Elliott, D. A. (2015). Forearm Range of Motion in *Australovenator wintonensis* (Theropoda, Megaraptoridae). *PLOS ONE*, *10*(9), e0137709. https://doi.org/10.1371/journal.pone.0137709

Xu, X., Han, F., & Zhao, Q. (2015). Homologies and homeotic transformation of the theropod 'semilunate' carpal. *Scientific Reports*, *4*(1), 6042. https://doi.org/10.1038/srep06042